

Summary of Propeller Research

Prof Antonio Filippone et al.

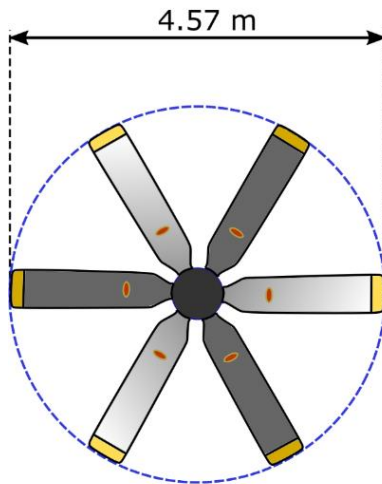
School of Engineering

The University of Manchester

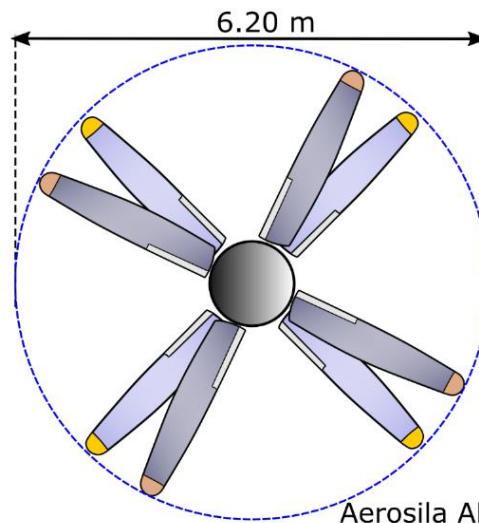
a.filippone@manchester.ac.uk

(June 2025)

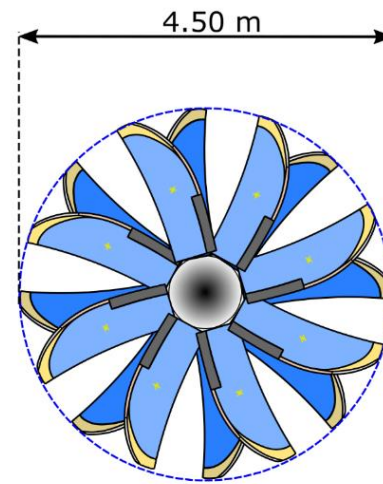
Propeller Geometries



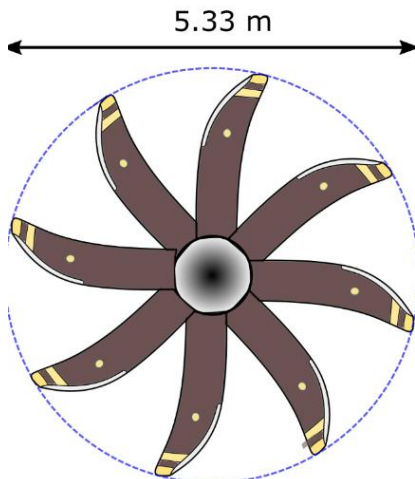
Hamilton AD-8664



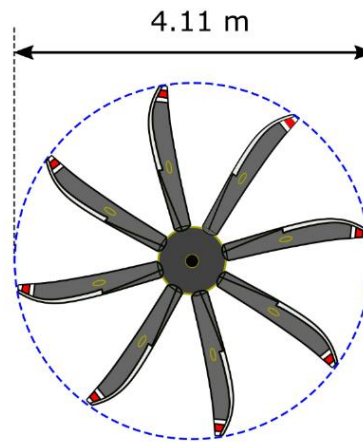
Aerosila AB-60



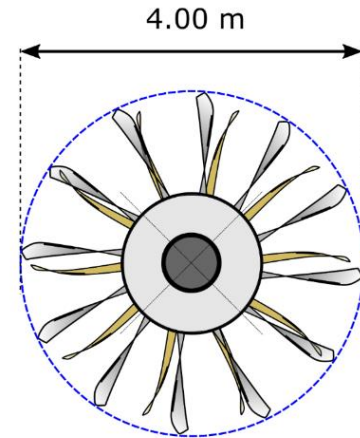
Aerosila SV-27



Ratier-Figeac FH386



Hamilton-Sundstrand NP2000



Safran Open Rotor

Summary of this Seminar

PART I

- Unequal blade-spacing propellers

PART II

- Multi-Rotor Flow Modelling

Background



Usov D., (2022), H-135 tail fenestron



Unknown, Piper J-3 Cub with the Everell single-blade propeller, www.quora.com



Verver G., (2012), AH-64 tail rotor

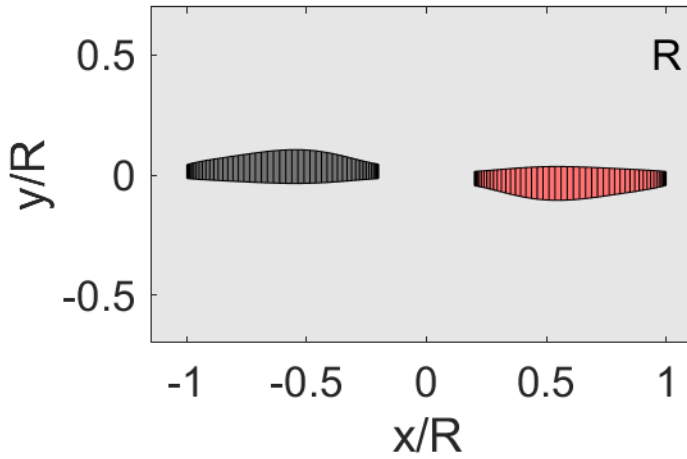
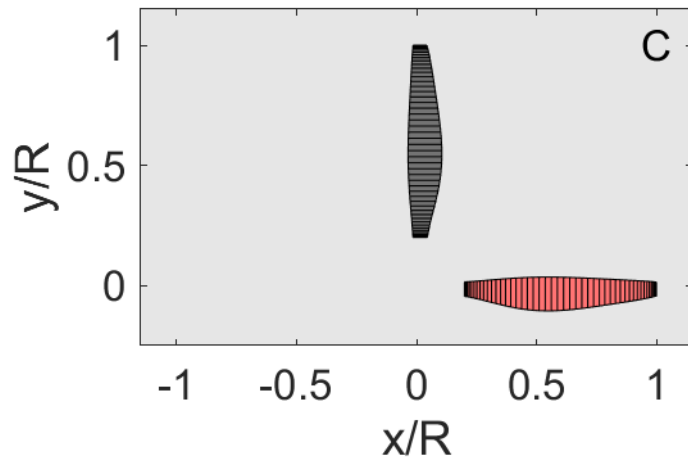
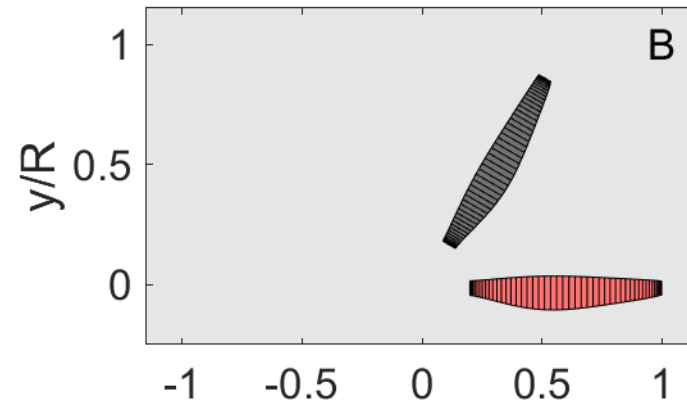
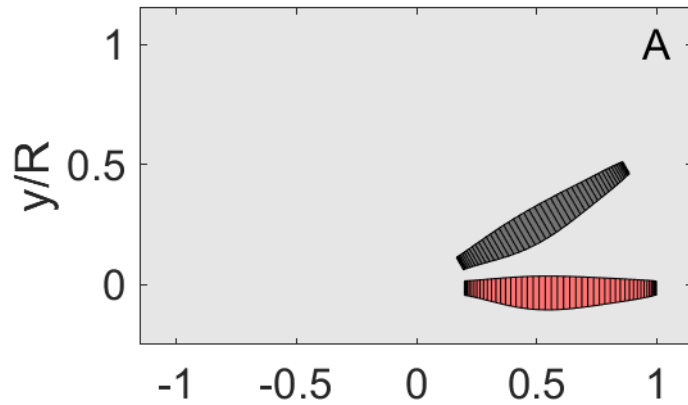


Rober M., (2023), Zipline propeller



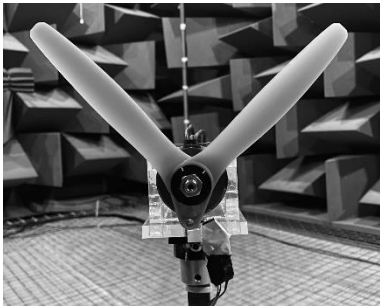
Usov D., (2023), Bolkow Bo-103 main rotor

Propellers with uneven blade spacing



Asymmetric propeller schematics.

Timeline



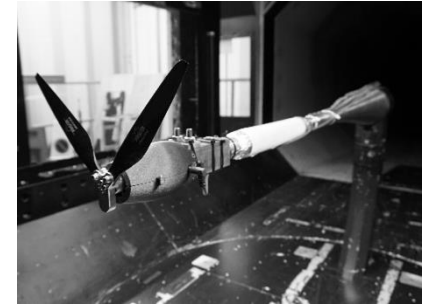
March 2024



June 2024



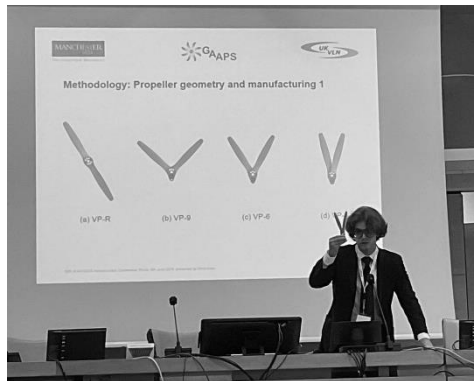
September 2024



October 2024



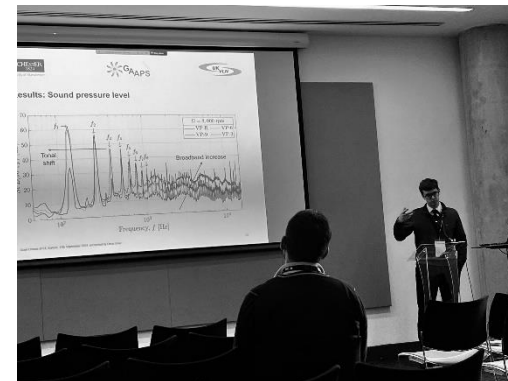
June 2024



July 2024



September 2024



Manufacturing: Propeller set



(a) VP-R



(b) VP-9

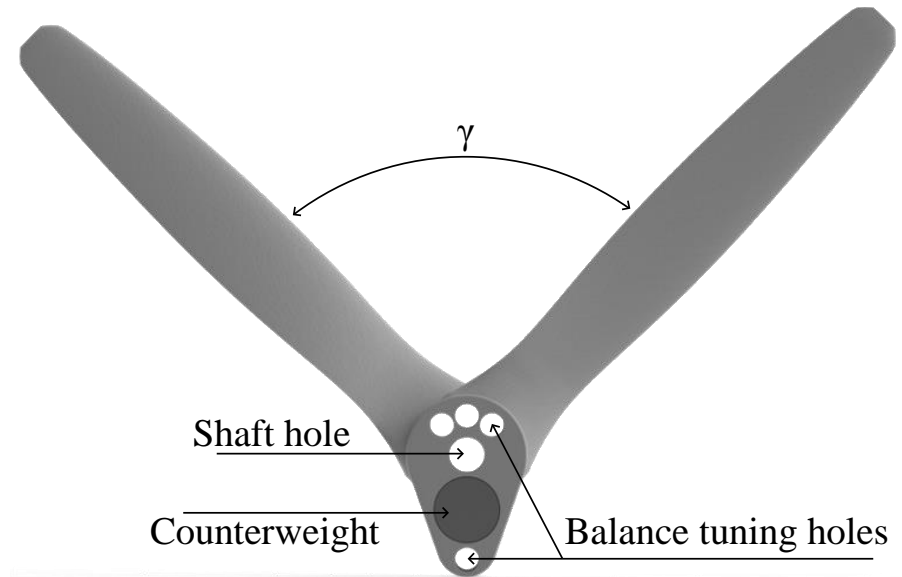


(c) VP-6



(d) VP-3

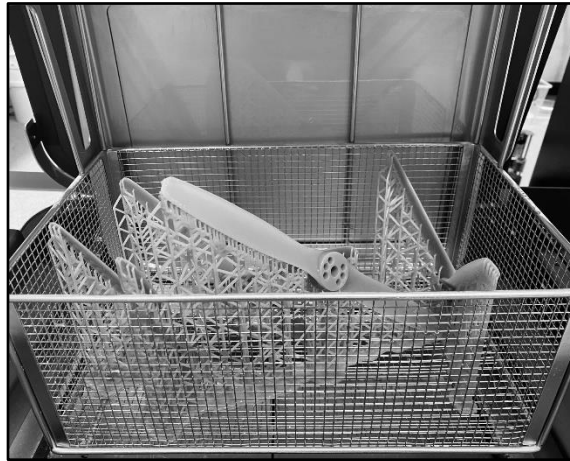
Prototype manufacturing: Geometry



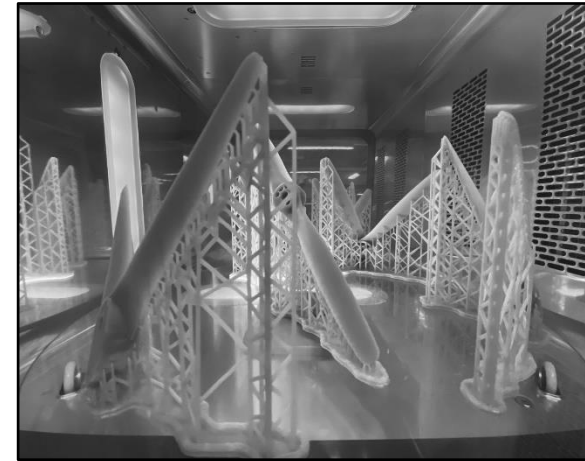
Prototype manufacturing: Process



(a) SLA printing

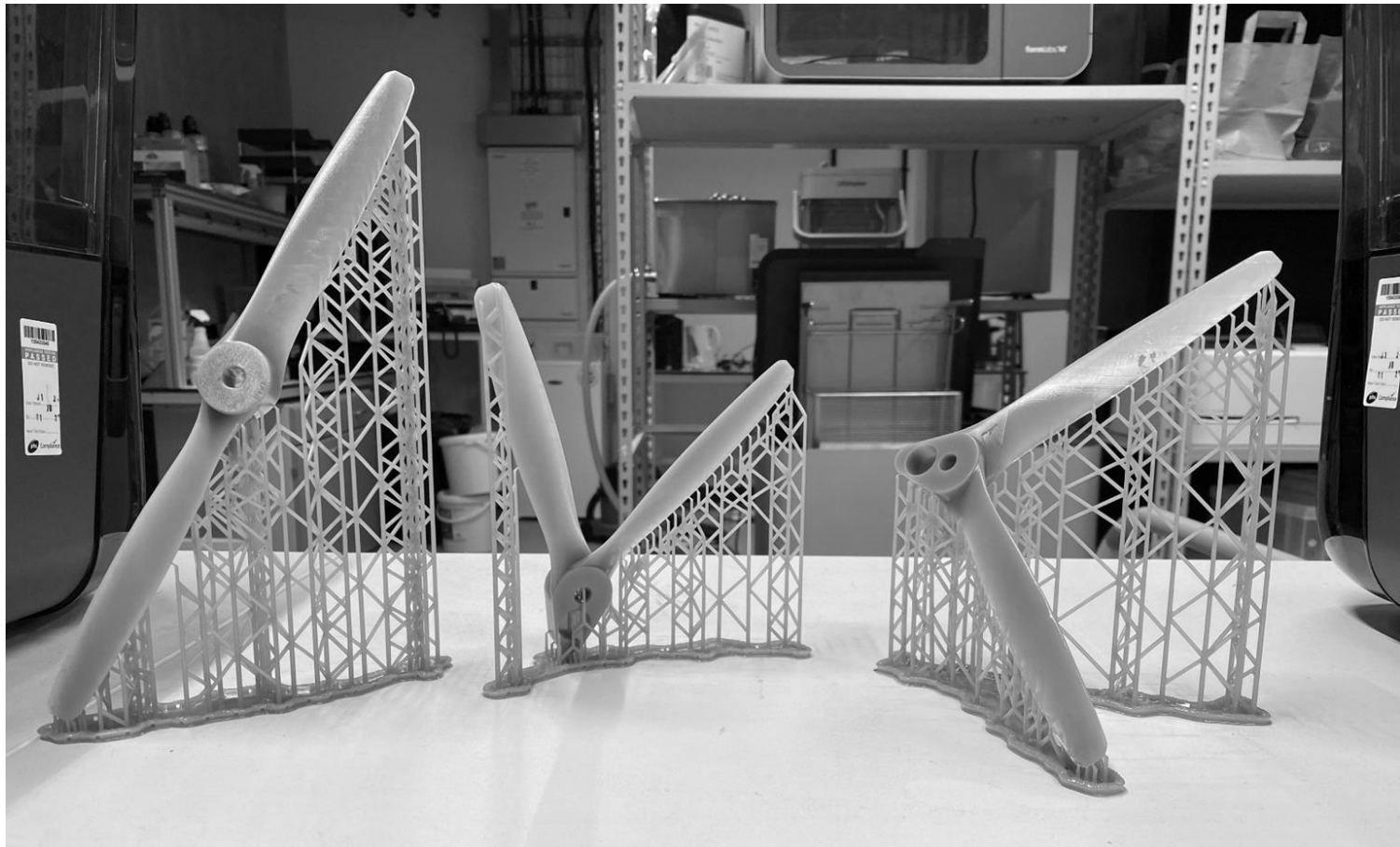


(b) IPA wash



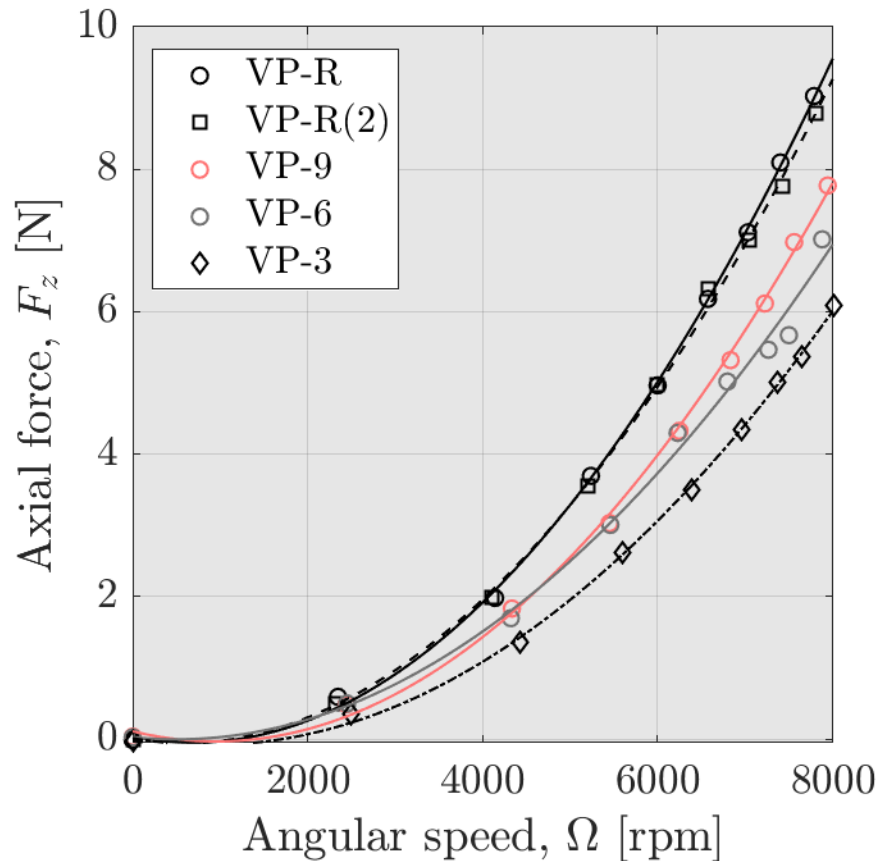
(c) UV-temperature curing

Manufacturing: Printed parts

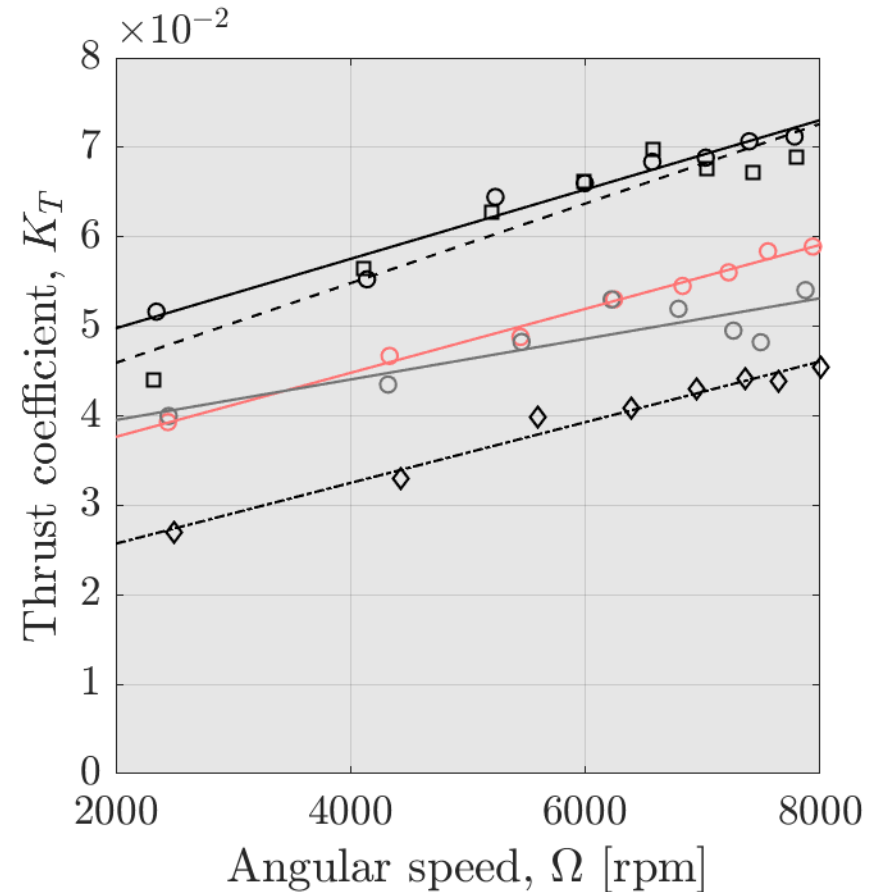


SLA printed, pre-processed propellers.

Preliminary acoustic measurements

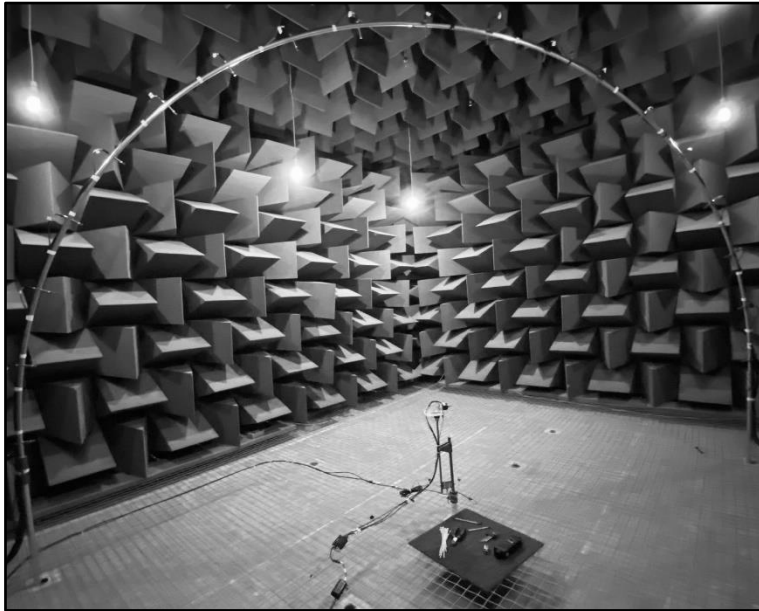


(a) Experimental thrust

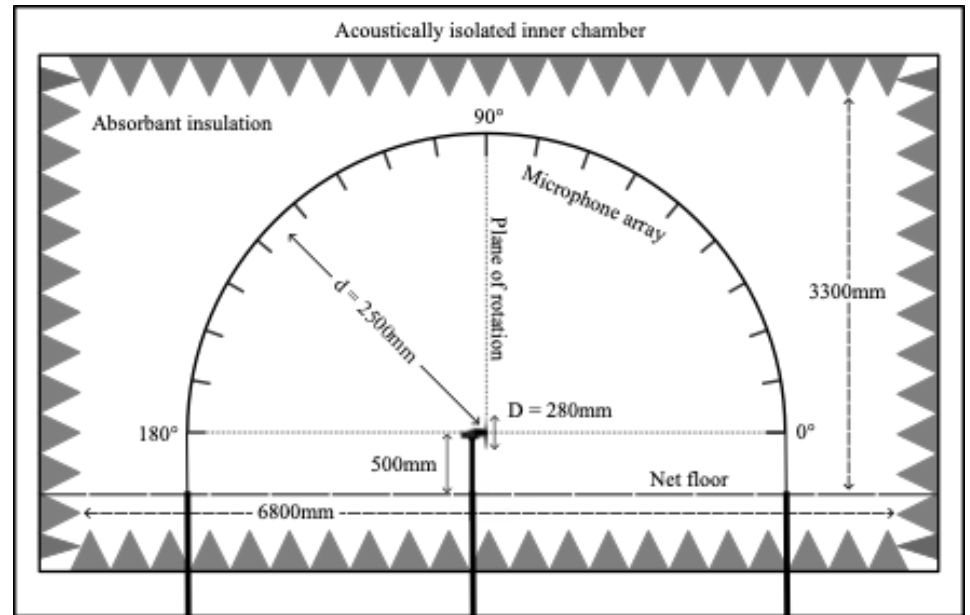


(b) Experimental Thrust coefficient

Anechoic chamber



(a) Microphone array



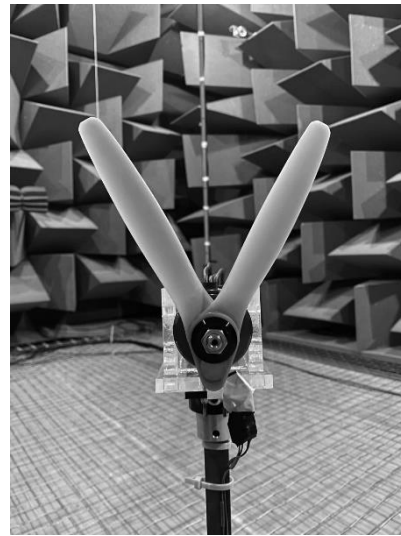
(b) Anechoic chamber

- Background: -12 dBA
- Facility time scale: ~120 s
- Cut-off: 50 Hz
- Sampling: 50 kHz

Preliminary acoustic measurements



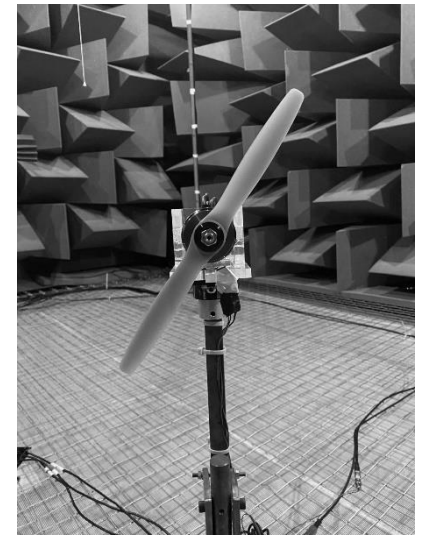
(a) VP-3.



(b) VP-6.



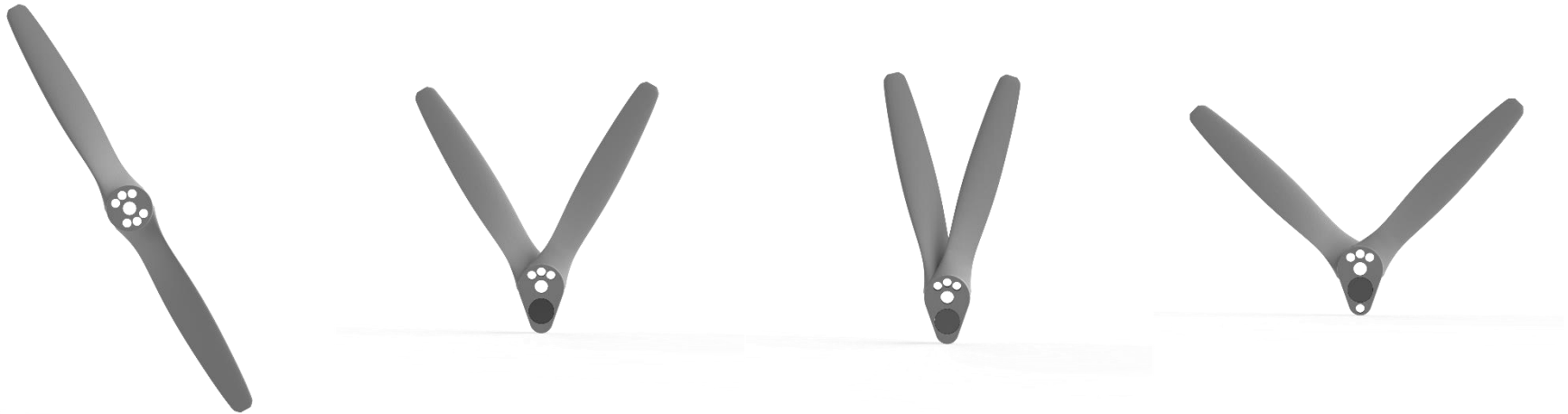
(c) VP-9.



(d) VP-R.

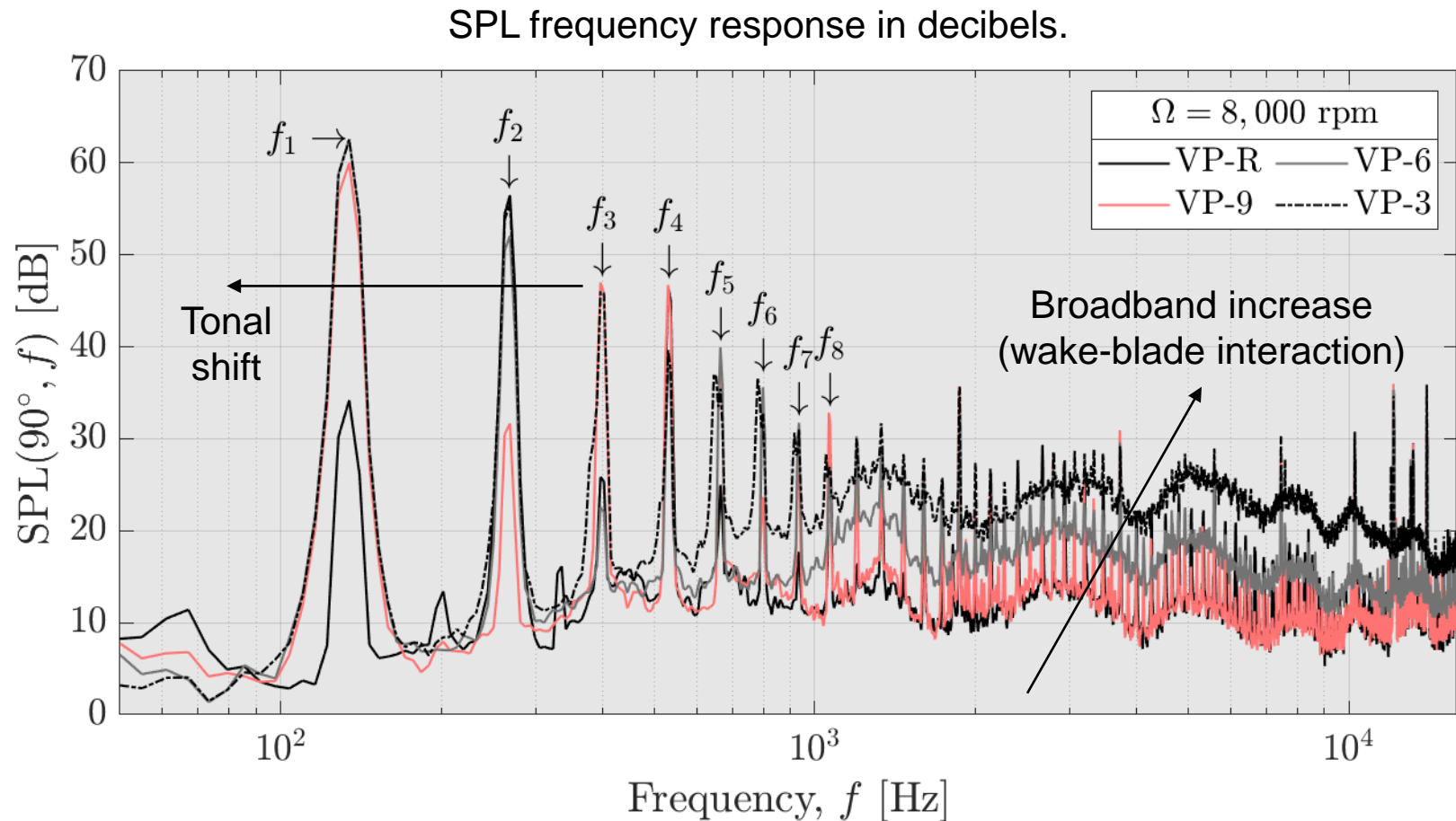
Preliminary acoustic measurements

Note: 8,000 rpm, diameter = 0.28 m, $M_{tip} = 0.35$, static propeller



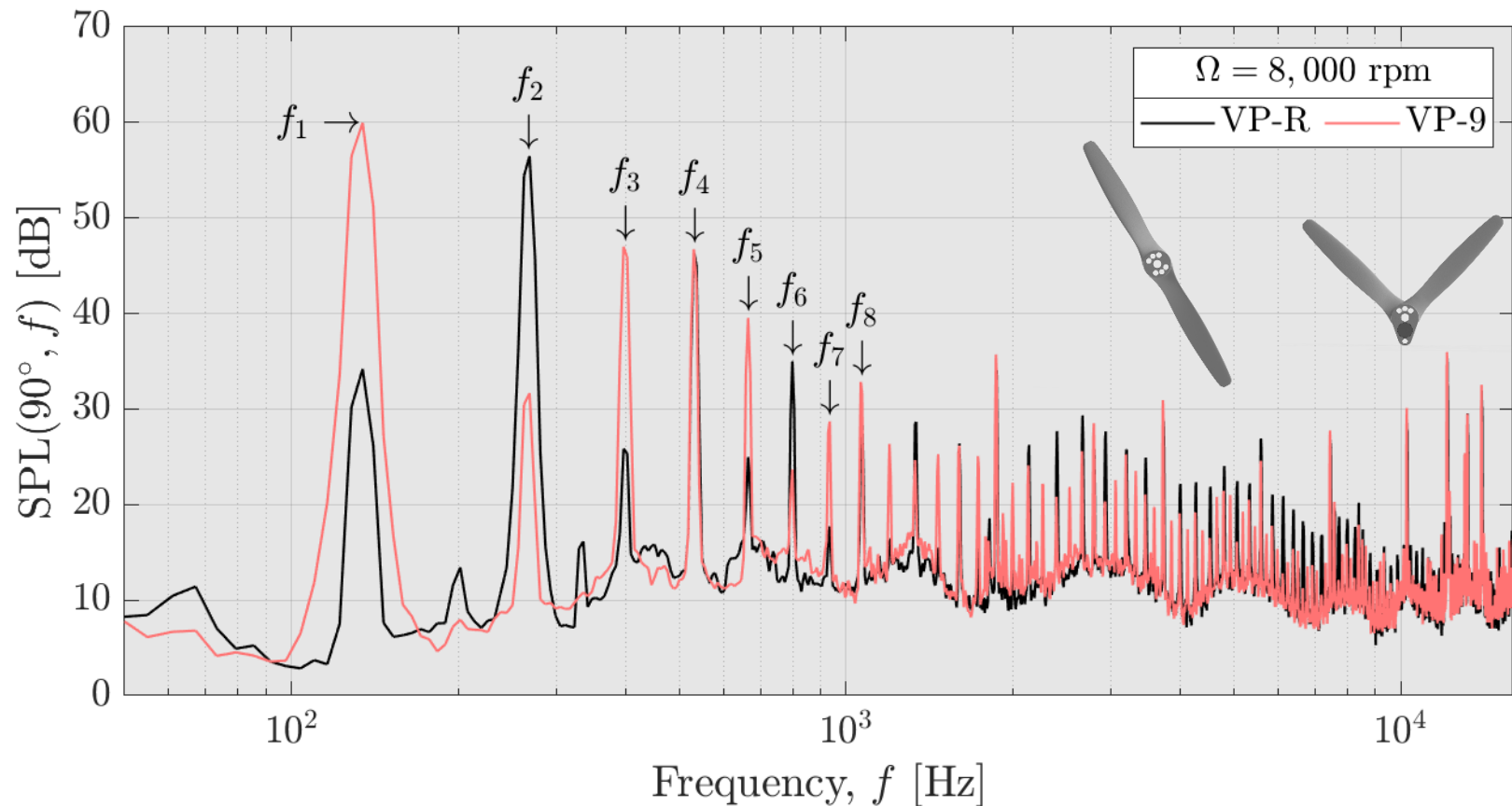
A	B	C	D
			

Preliminary acoustic measurements



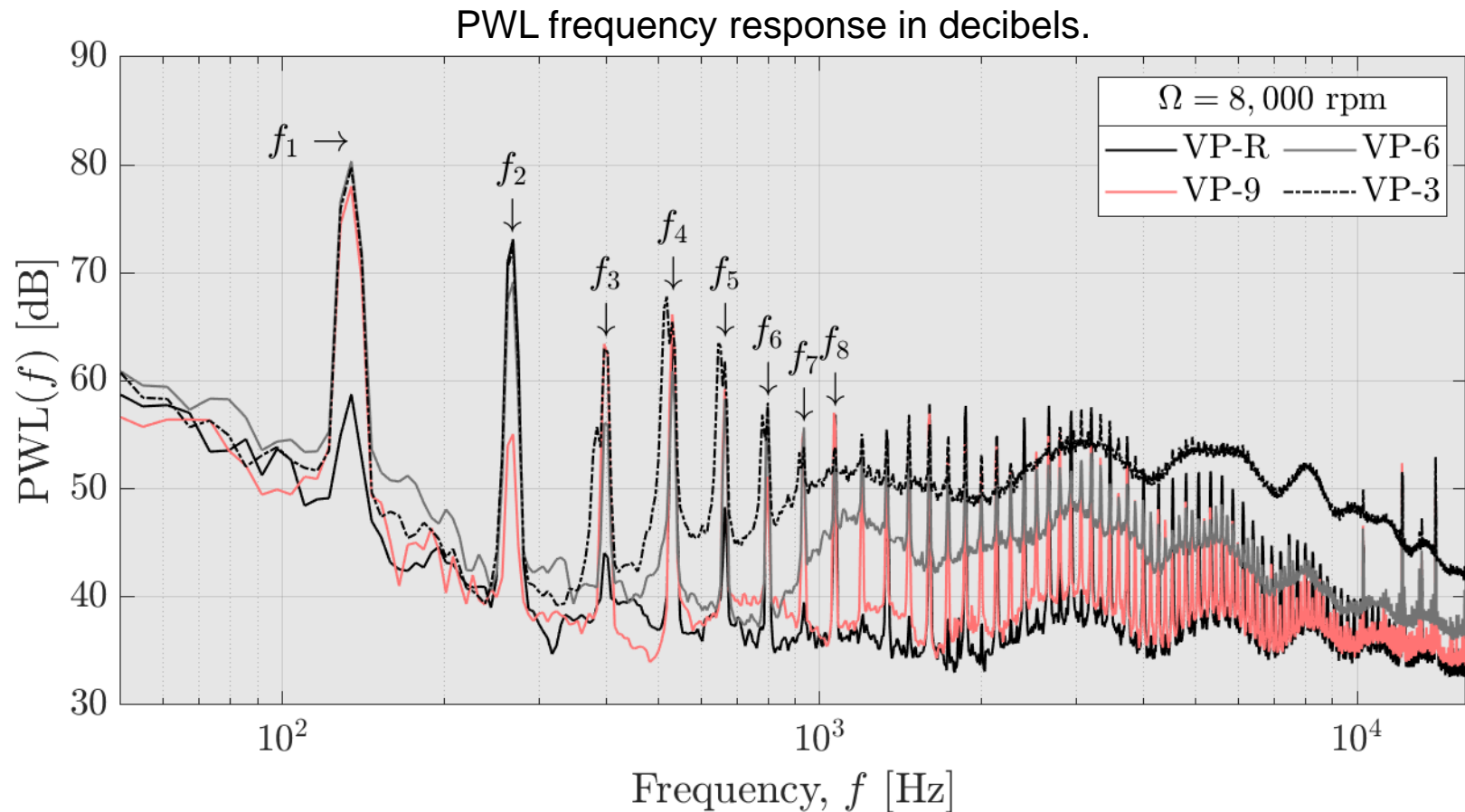
Acoustic measurements

SPL of VP-9 vs reference propeller

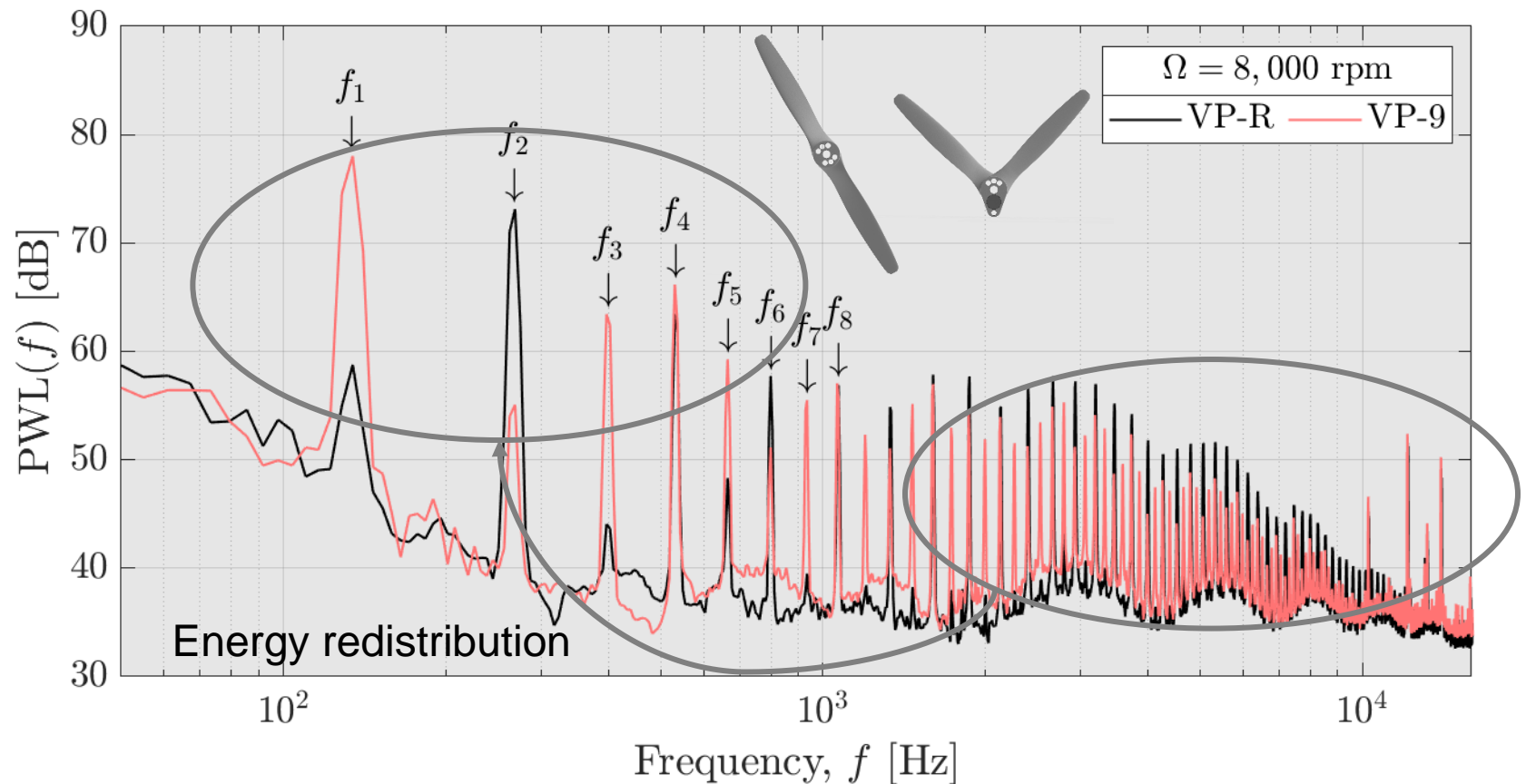


Acoustic measurements

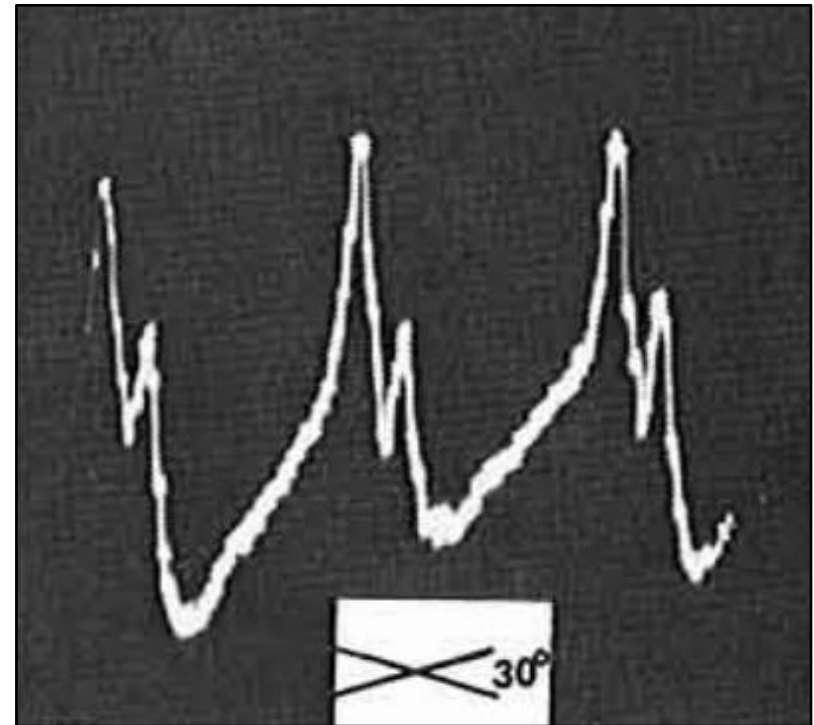
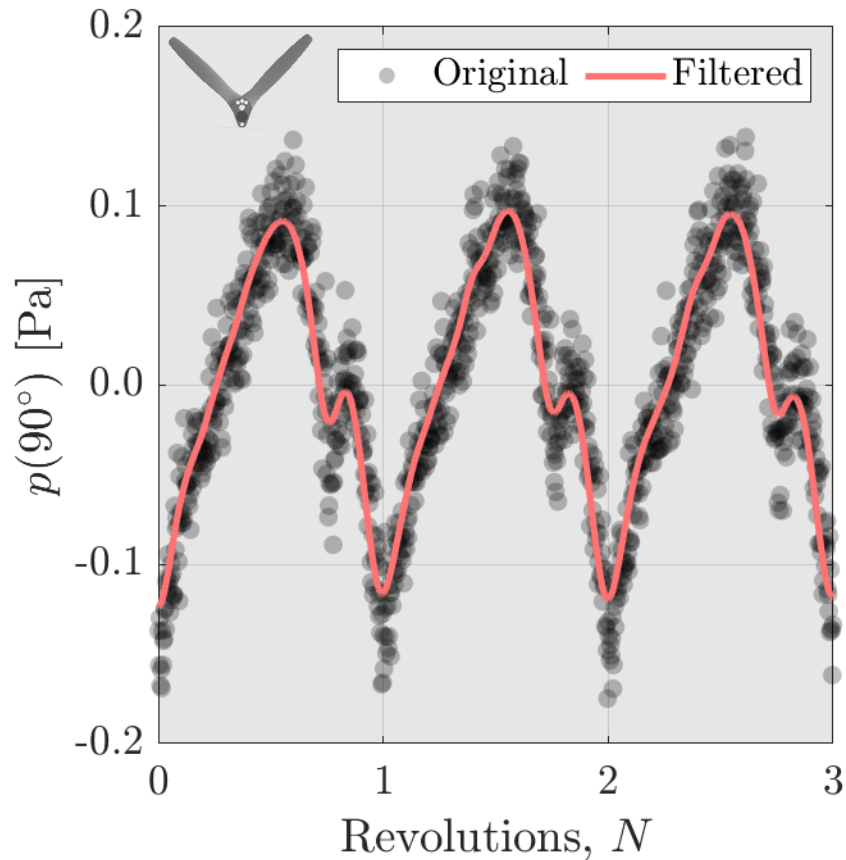
Power level (PWL)



Acoustic measurements: PWL VP-9



Acoustic measurements



Sonneborn and Drees, JAHS (1975)

Final Design: Geometry

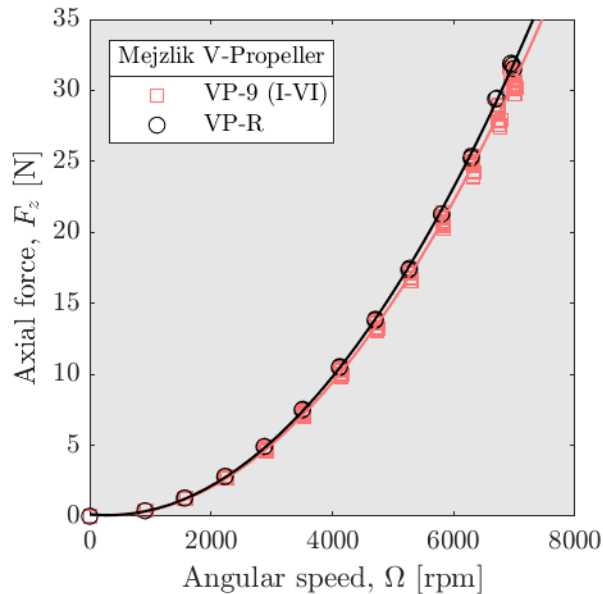


(a) VP-R

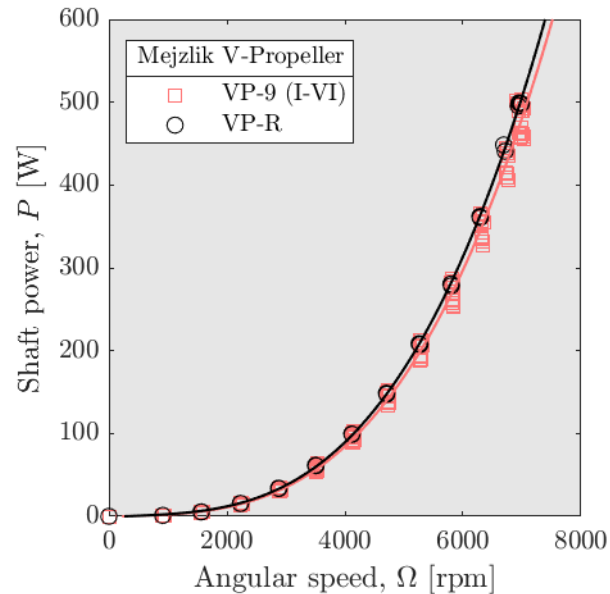


(b) VP-9

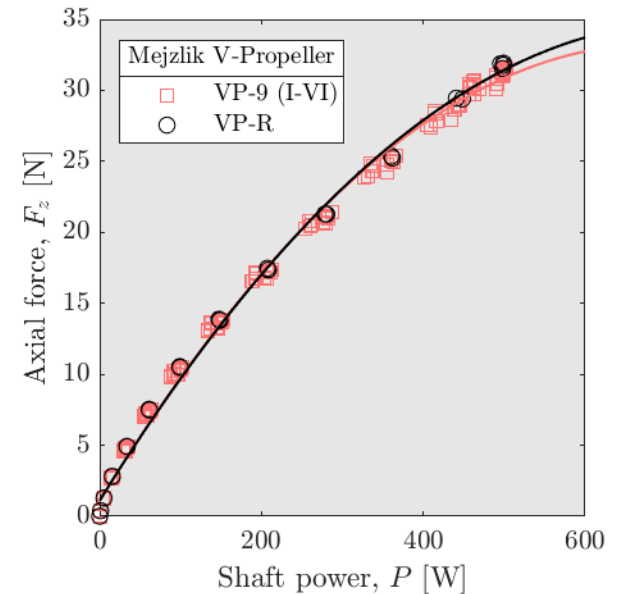
Final Design: *Static performance



(a) Thrust



(b) Torque



(c) Efficiency

*Data scatter represents six VP-9 propeller

Outdoor tests: Overview



(a) UAS with conventional propellers

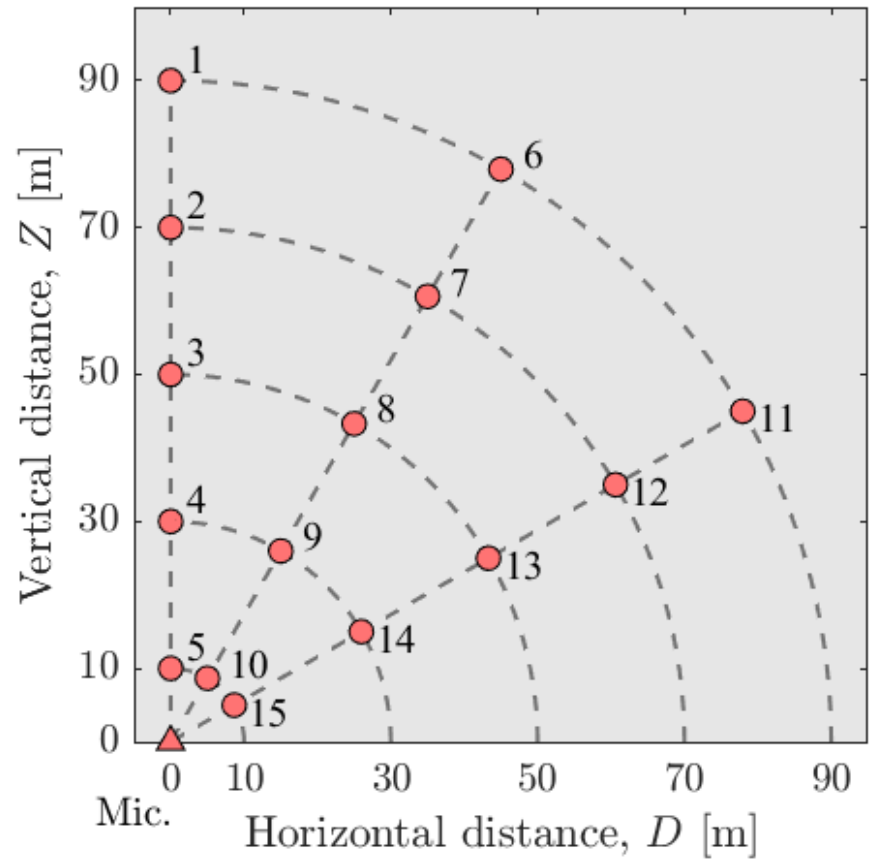


(b) UAS with asymmetric propellers

Outdoor test: Test Matrix



(a) Hover over the inverted microphone



(b) Visual test matrix

Outdoor test: Instrumentation

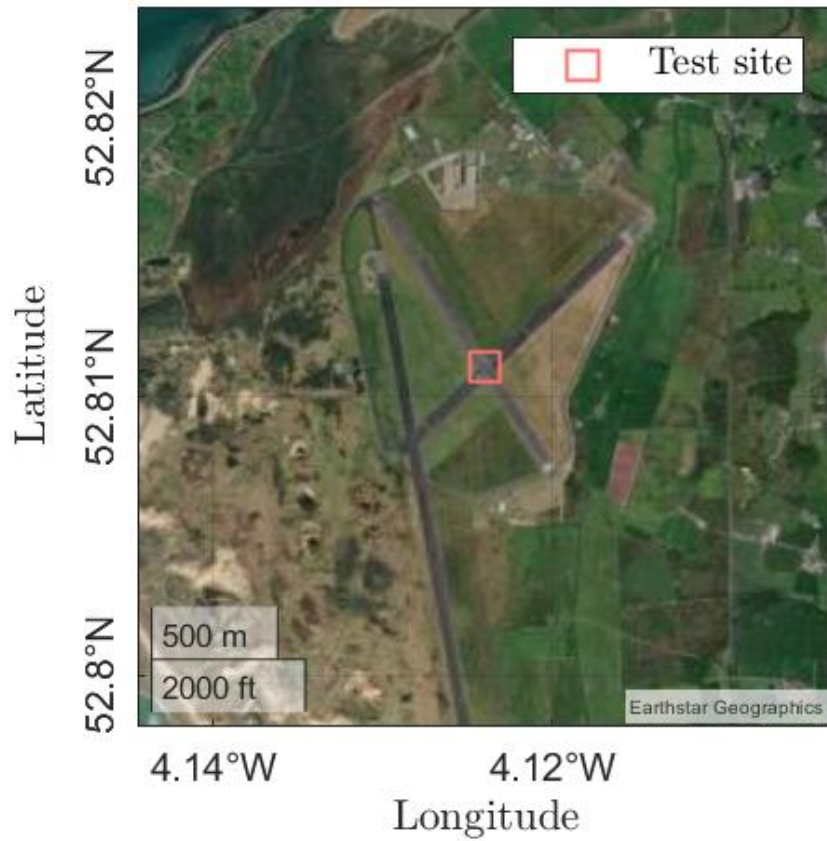


(a) Anemometer setup

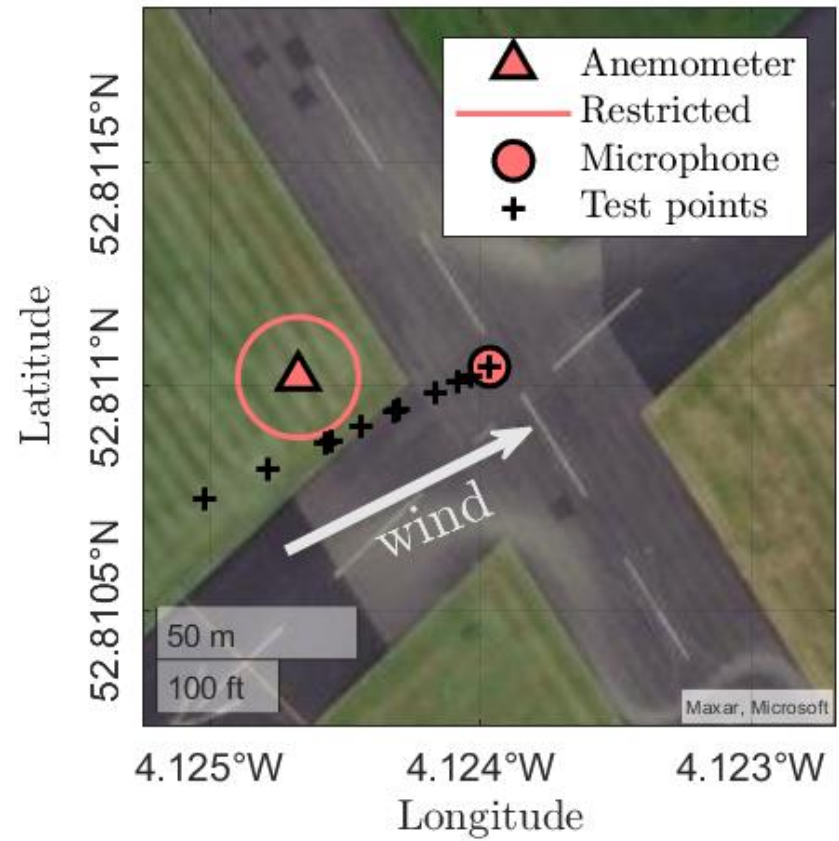


(b) Inverted microphone setup

Outdoor test: Site



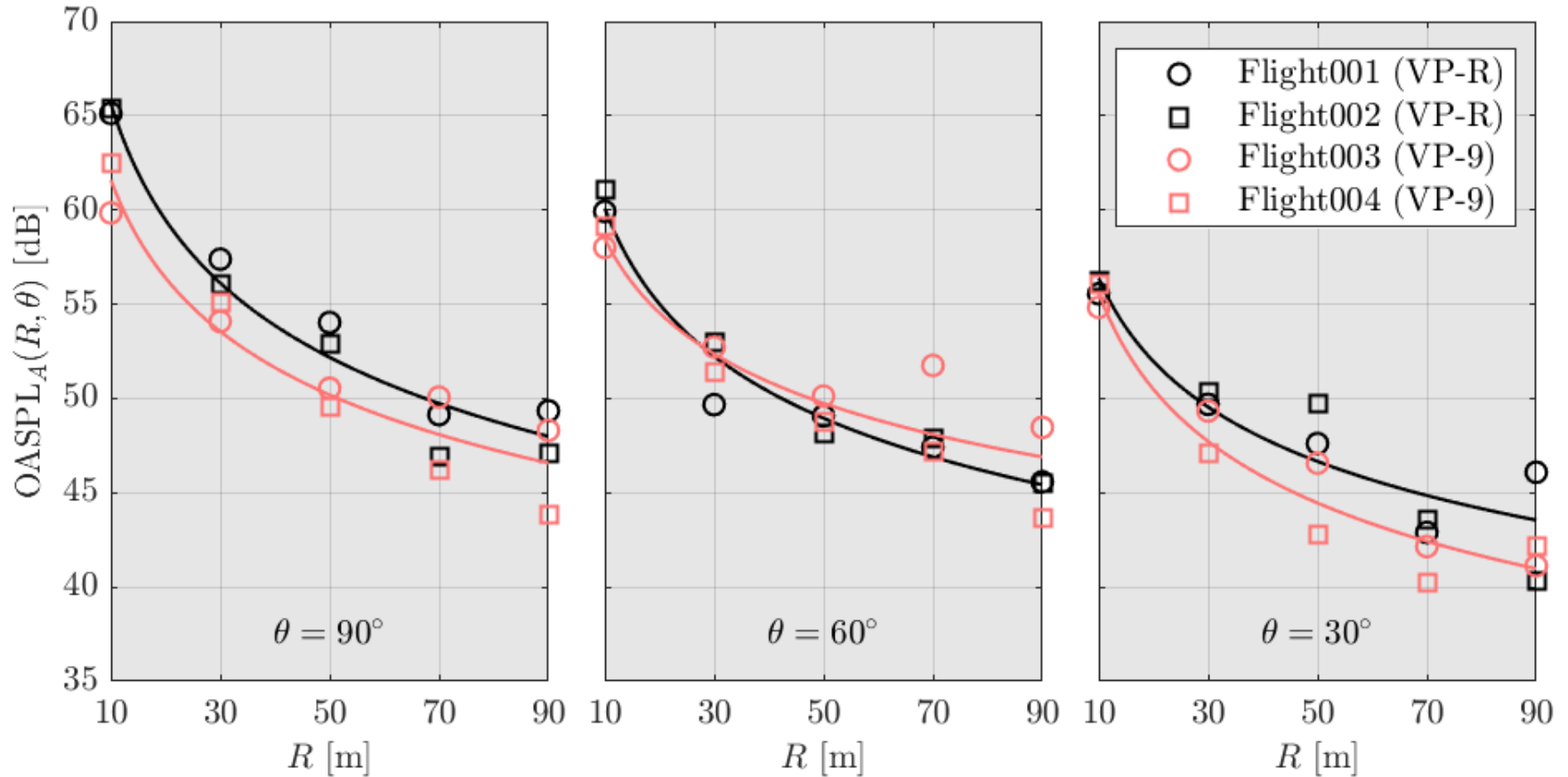
(a) Airfield



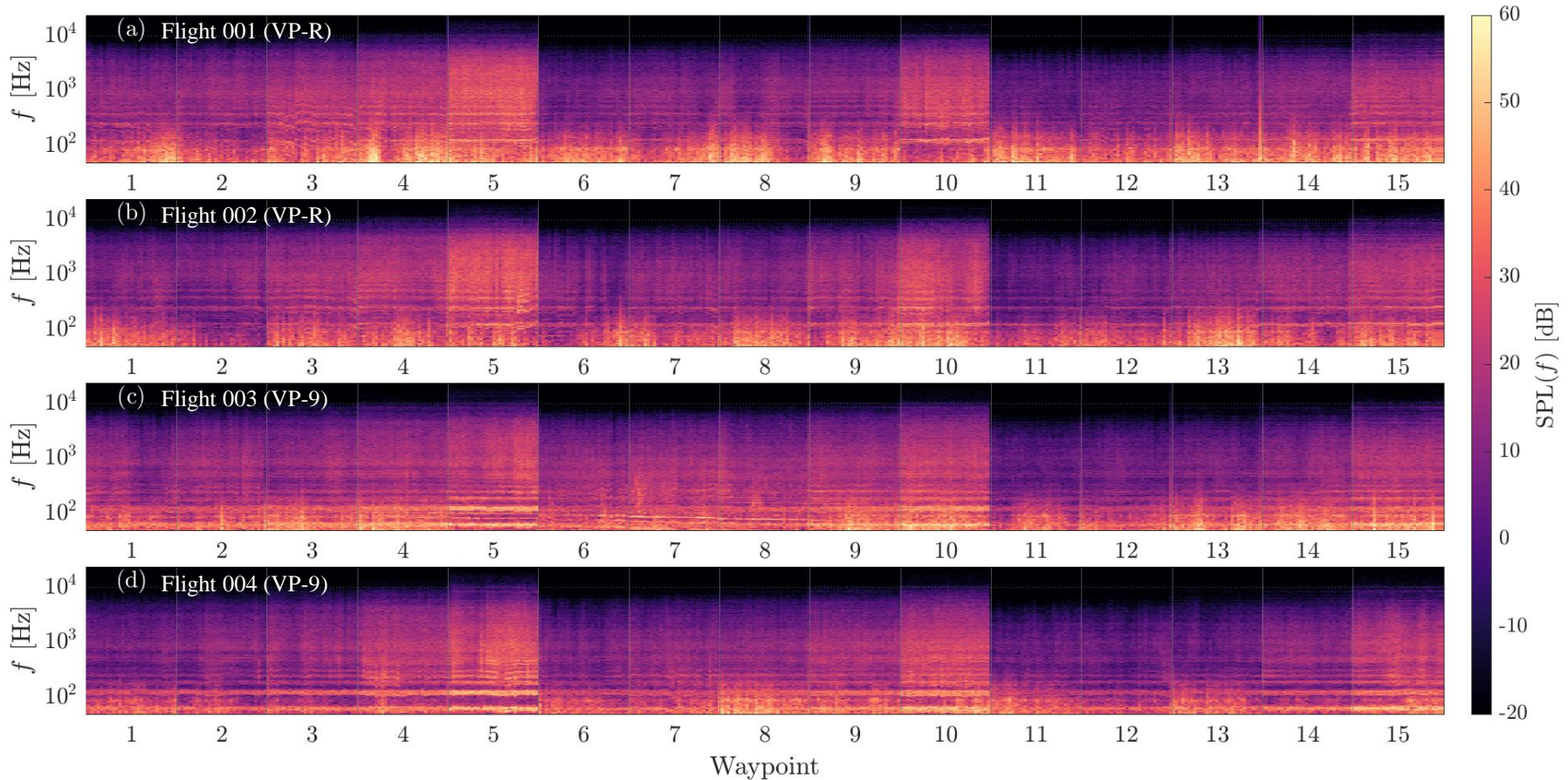
(b) Test site

Outdoor tests: OASPLA

Outdoor acoustic response, OASPLA

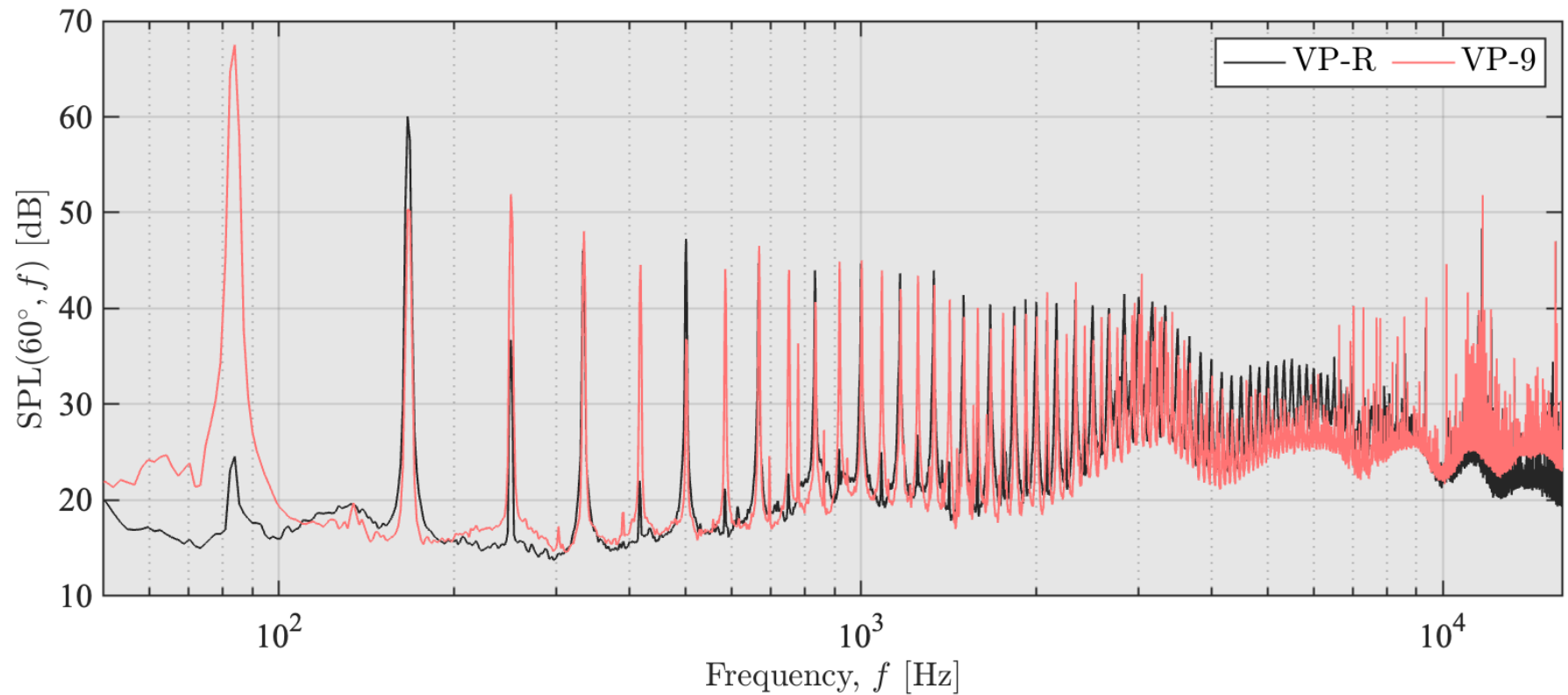


Outdoor tests: SPL Spectra



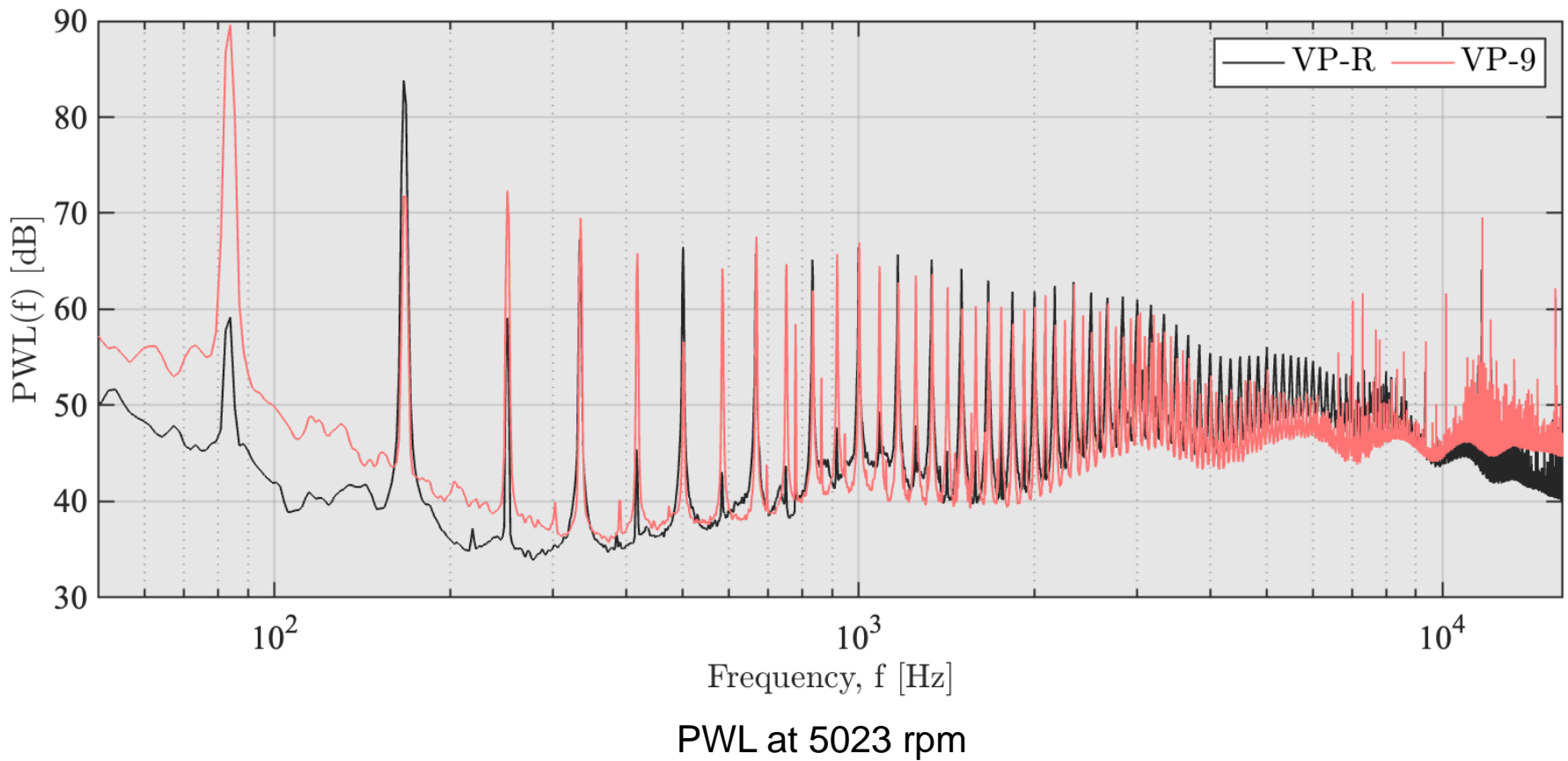
Outdoor acoustic response, SPL spectra.

Acoustic measurements: SPL



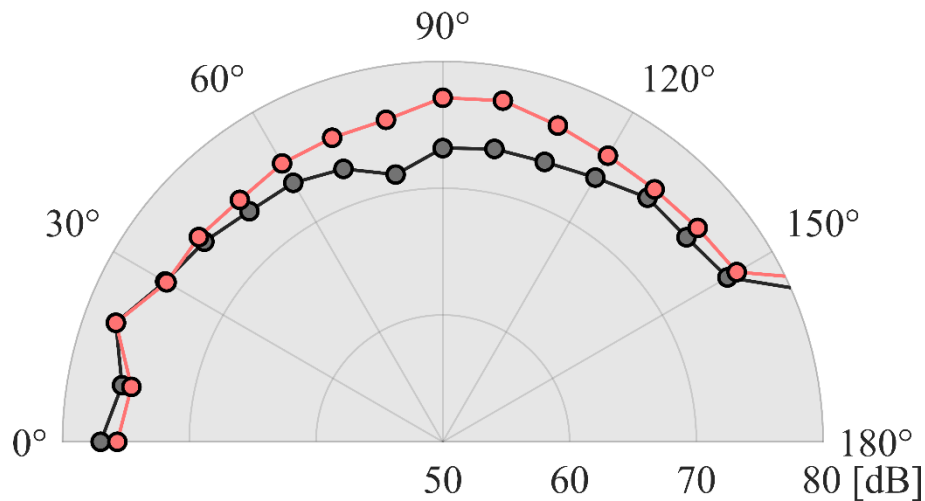
SPL at 60-degree emission angle and 5012 rpm

Acoustic measurements: PWL



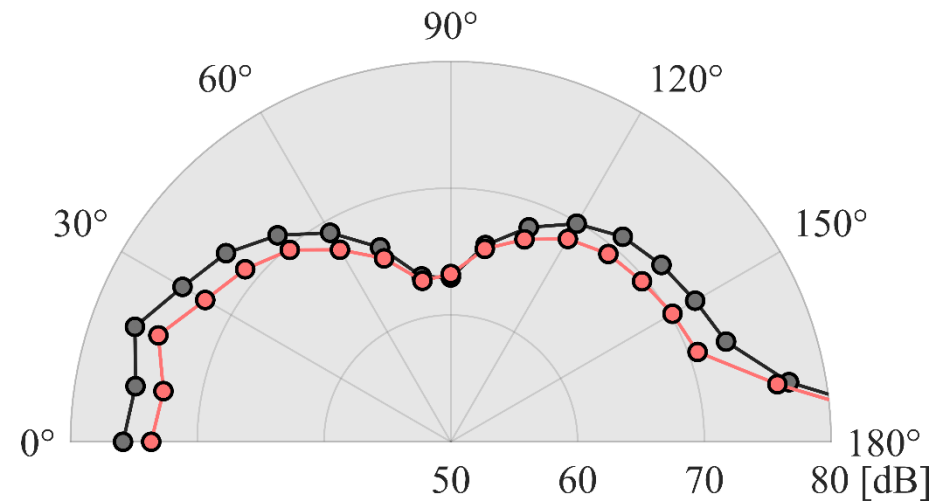
Acoustic measurements: Directivity

$\Omega = 5012 \text{ rpm}; f_b = 166.7 \text{ Hz}$
—●— VP-R —●— VP-9



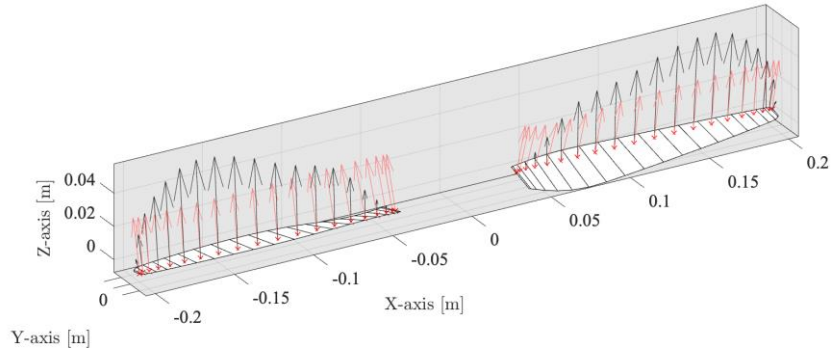
(a) OASPL

$\Omega = 5012 \text{ rpm}; f_b = 166.7 \text{ Hz}$
—●— VP-R —●— VP-9

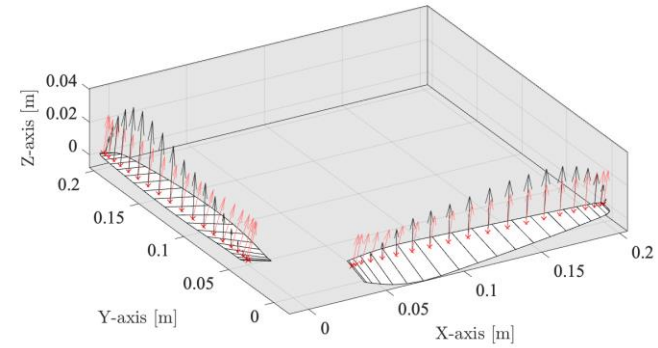


(b) OASPLA

Acoustic simulations: Validation 1



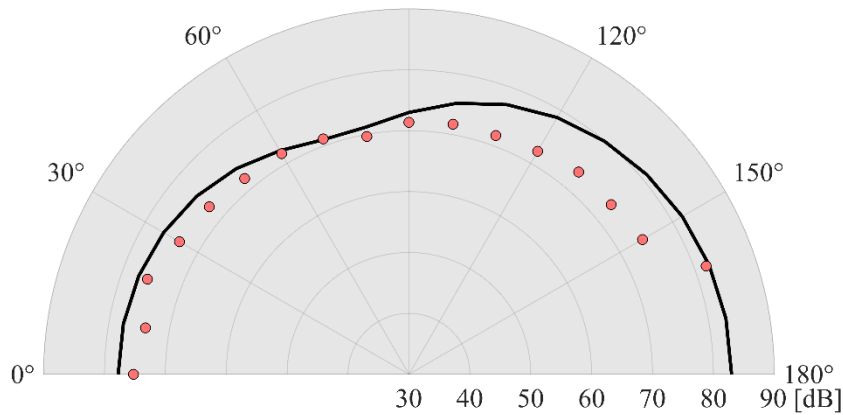
(a) VP-R



(b) VP-9



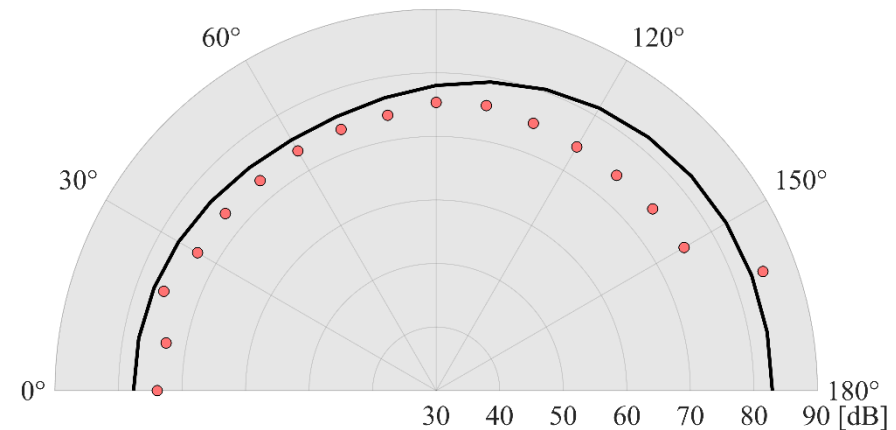
90°



(c) OASPL VP-R

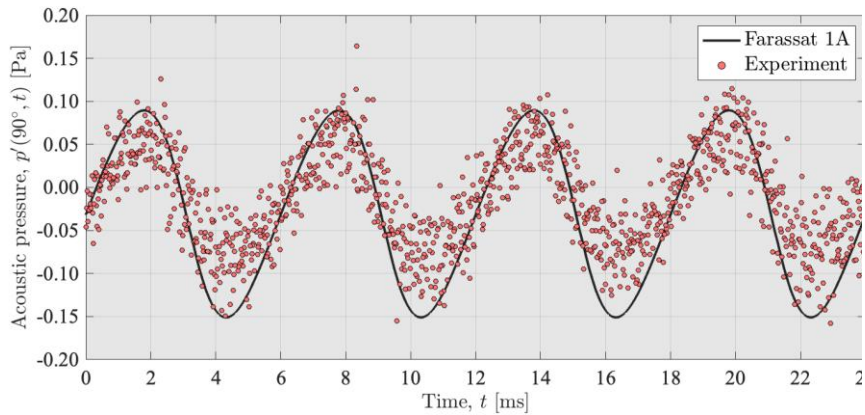


90°

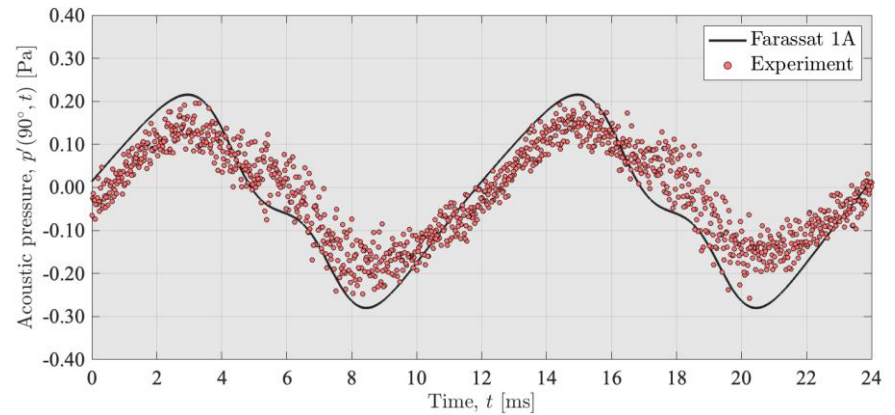


(c) OASPL VP-9

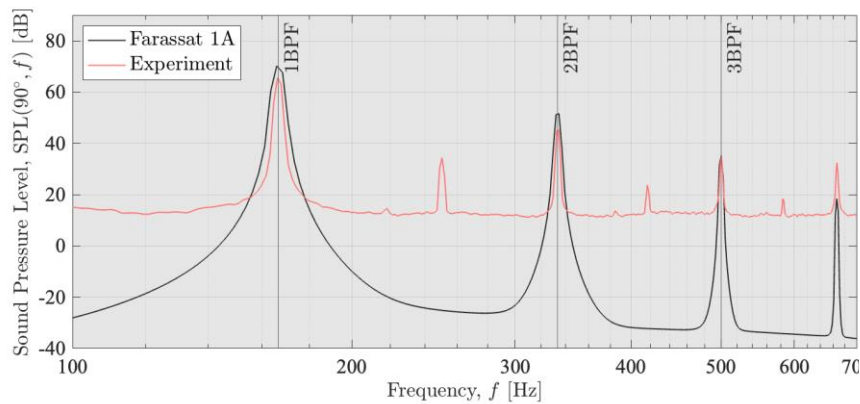
Acoustic simulations: Validation 2



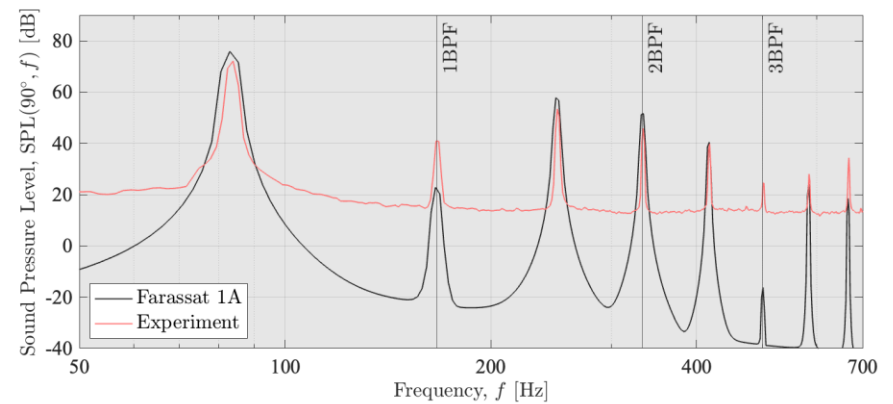
(a) Pressure waveform VP-R



(b) Pressure waveform VP-9



(b) SPL VP-R



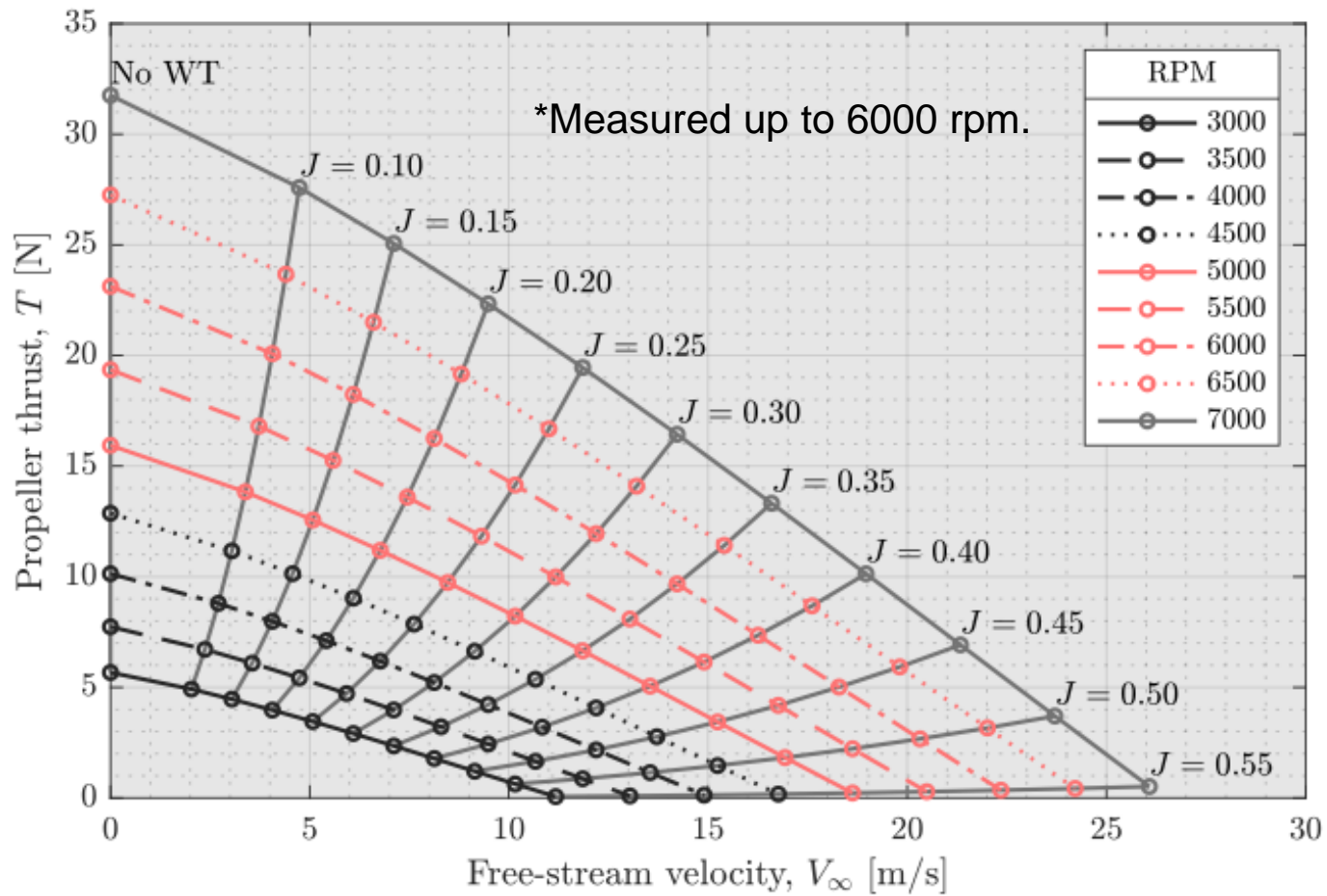
(b) SPL VP-9

Wind tunnel measurements: Setup



Wind tunnel tests, propeller rig setup.

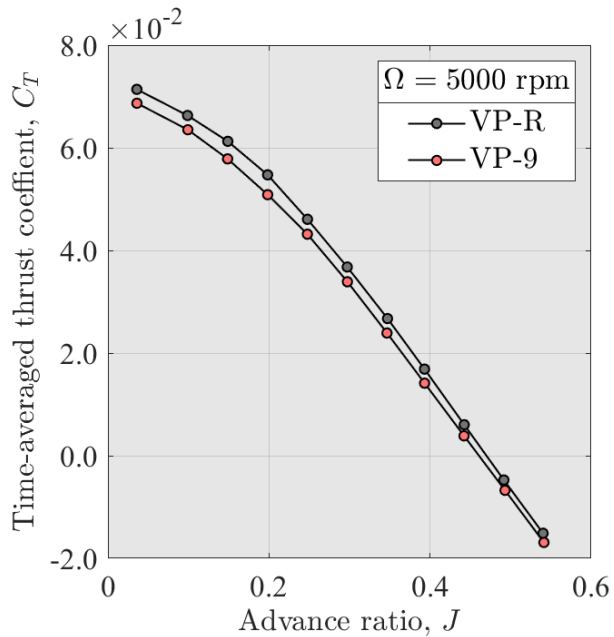
Wind tunnel measurements: Test matrix



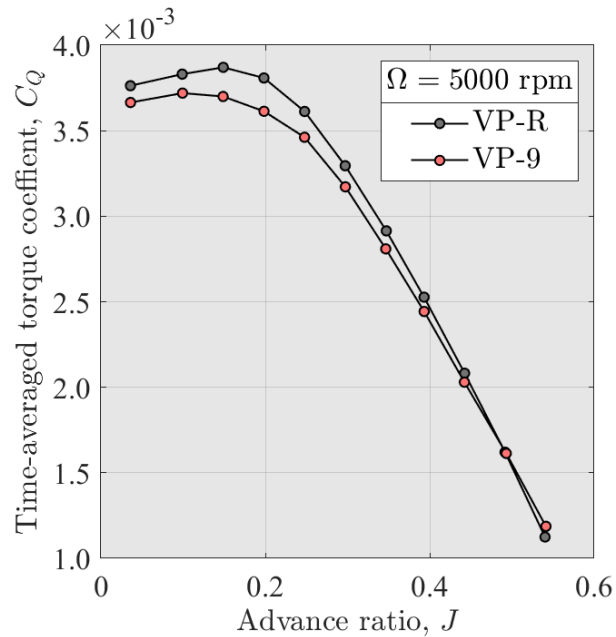
Outcomes

- Propeller design to be licensed to
 - Mežlik Propellers s.r.o.
 - Brno, Czech Republic, 615 00

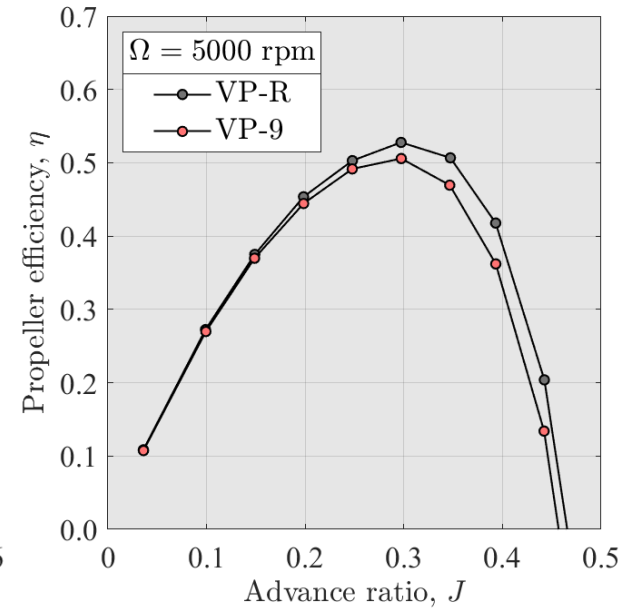
Wind tunnel measurements



(a) Wind tunnel tests, C_T .



(b) Wind tunnel tests, C_Q .



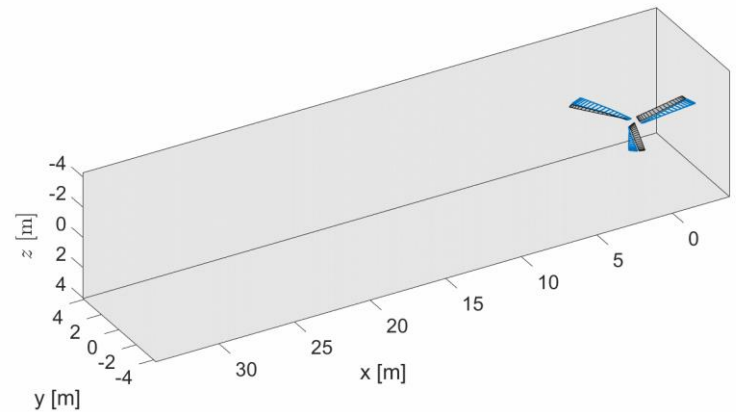
(c) Wind tunnel tests, η .

PART II

Use of Proper Orthogonal
Decomposition for Complex Flows

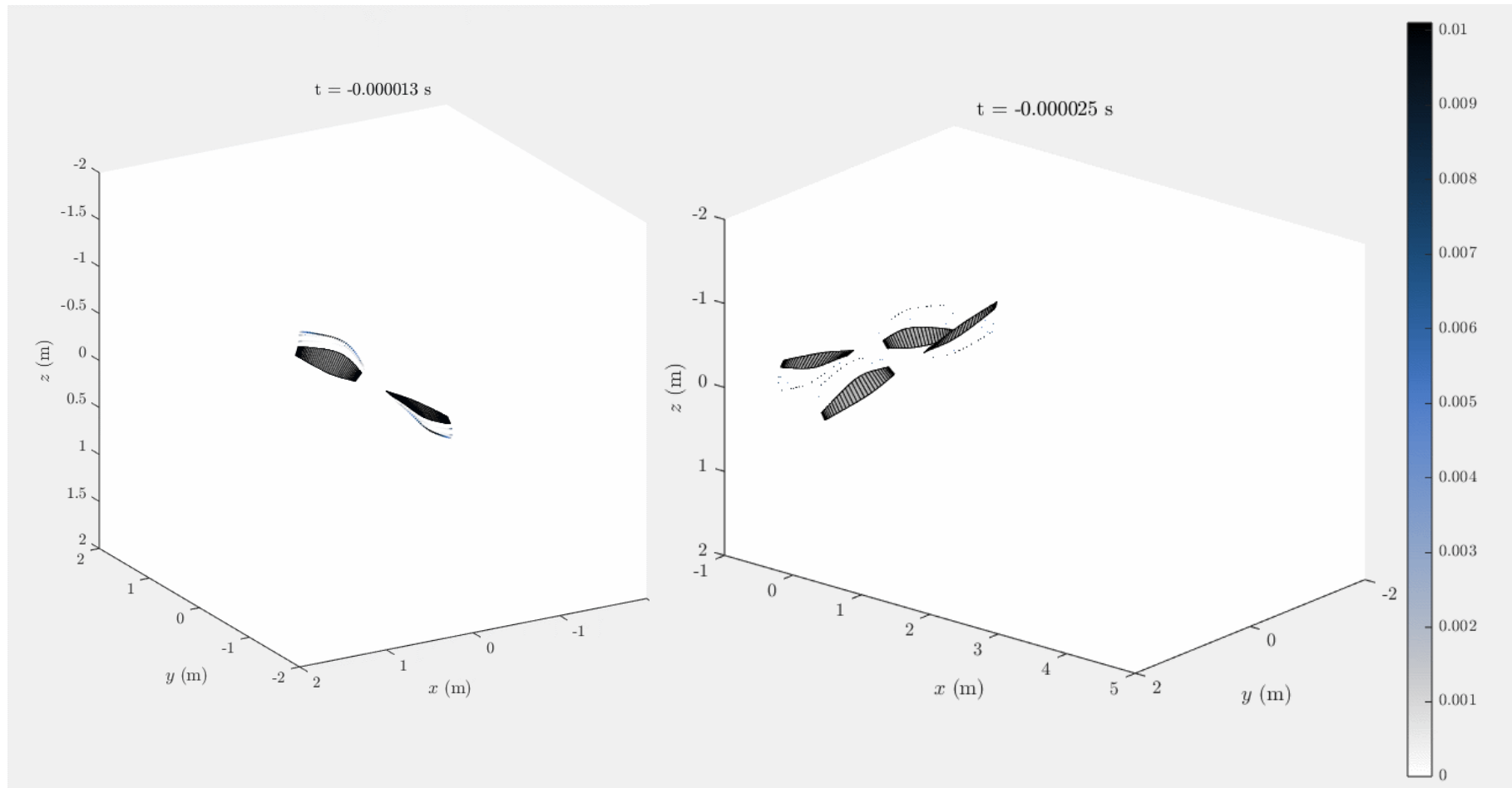
Aerodynamics Modelling

- Single- contra-rotating propellers
- Models
 - Dynamic inflow
 - Lifting lines
 - Vortex particle methods
 - (Analytical models)
 - Steady/unsteady analysis
 - Change of shaft angle
- Flight mechanics coupling



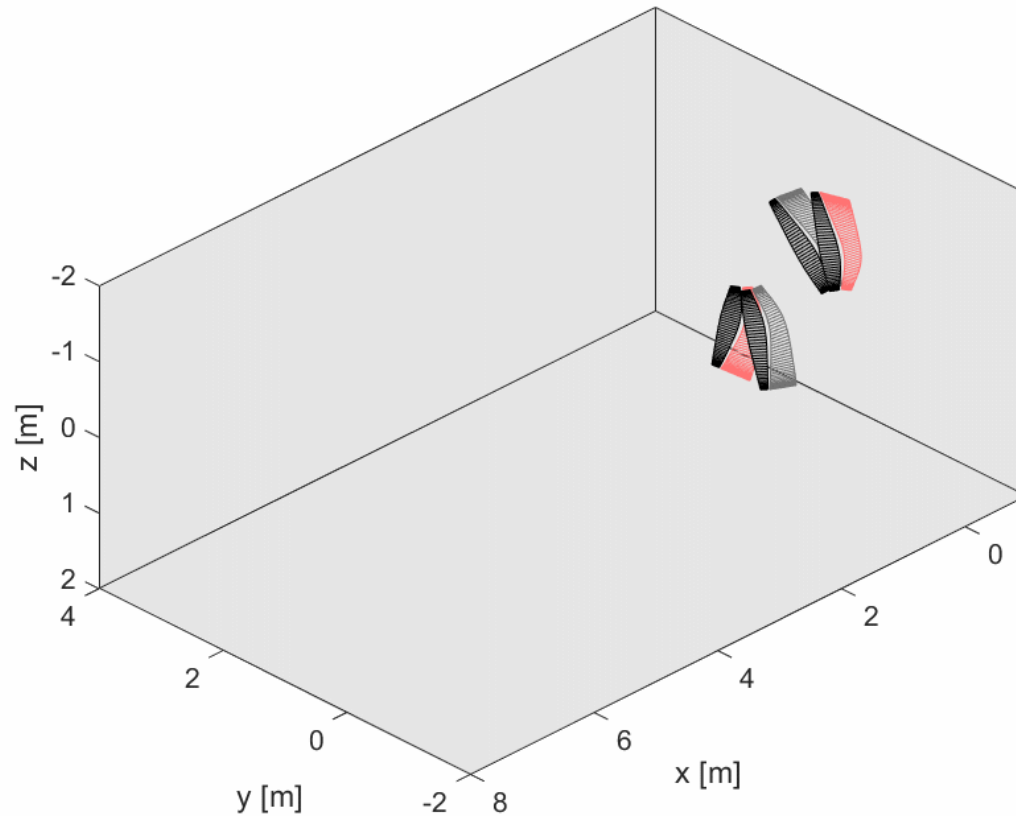
Vortex Theory: Free Wakes

- Hartman propeller and contra-rotating propeller



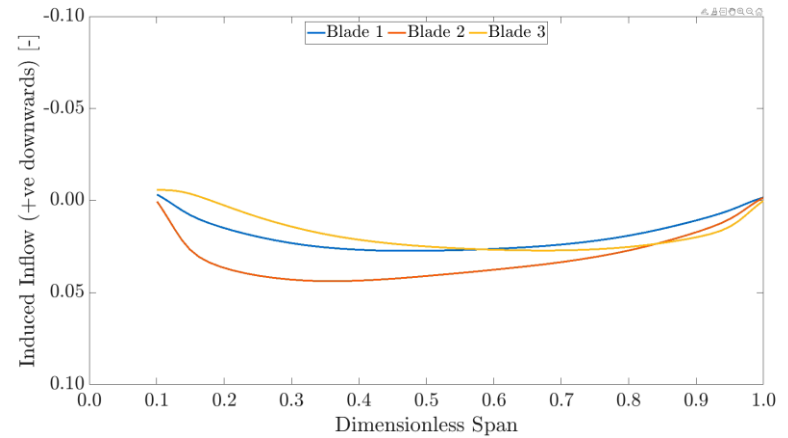
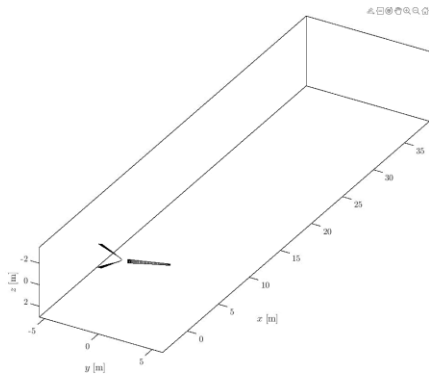
Exotic Propellers

- Unequal blade spacing, contra-rotating, axial flight



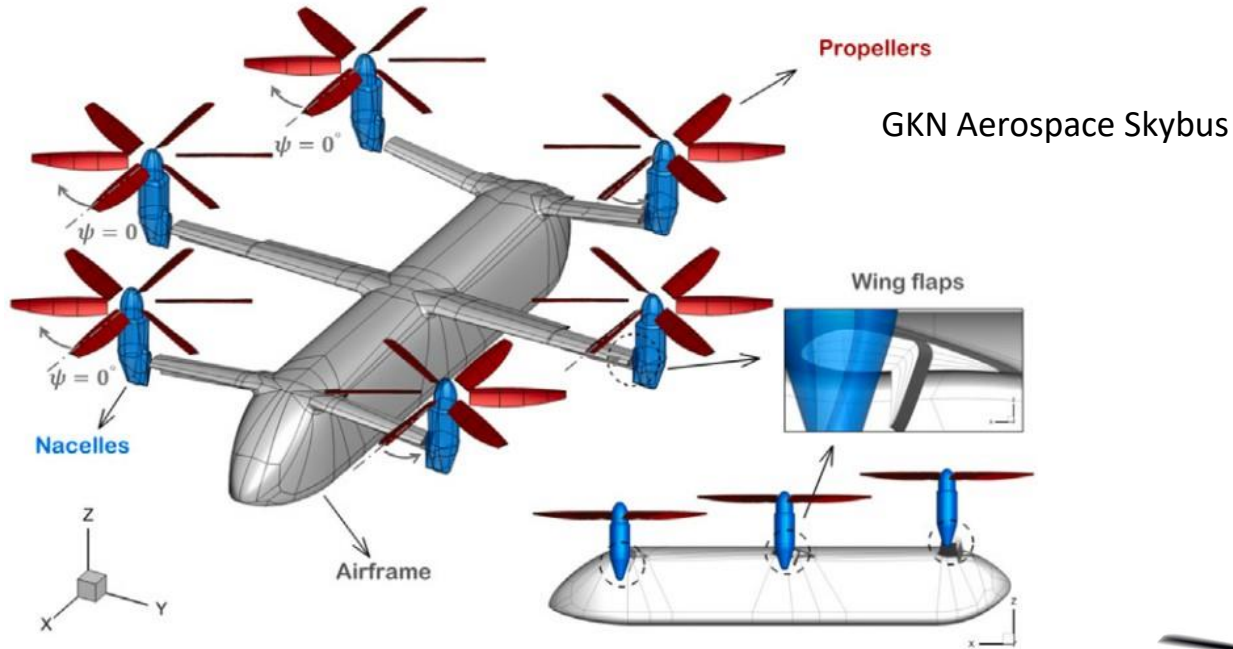
Rotor Inflow Transient

- Free flight



Motivations

- Small and large electrically-powered VTOL



Sora Aviation S-1 prototype

Industrial Landscape

- Significant interest in multi-rotor aircraft for eVTOL

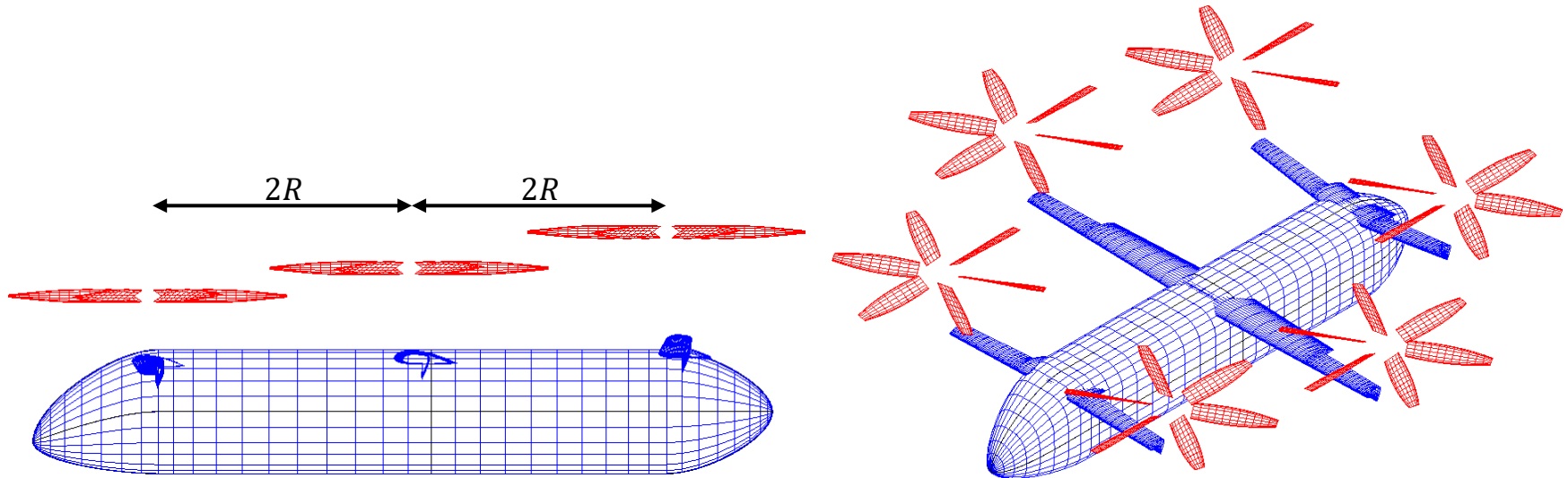


Motivation for vortex particle method

- New generation of eVTOL concepts reliant on multiple rotors and lifting surfaces
- CFD unavoidable in the detailed design phase
- Faster tools are more suited to conceptual design
- Important to assess the capabilities of mid-fidelity tools
- To correctly resolve interactional flow physics early

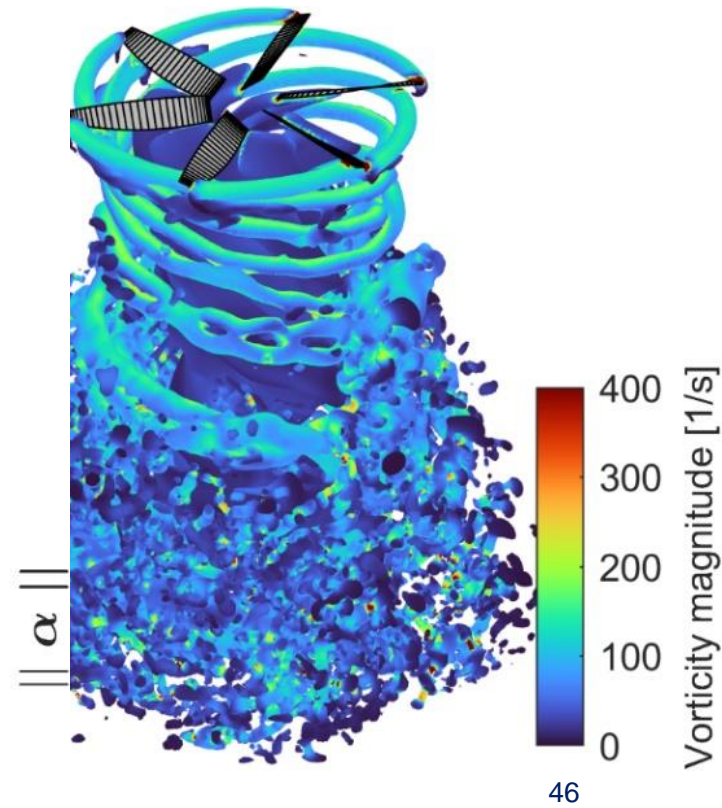
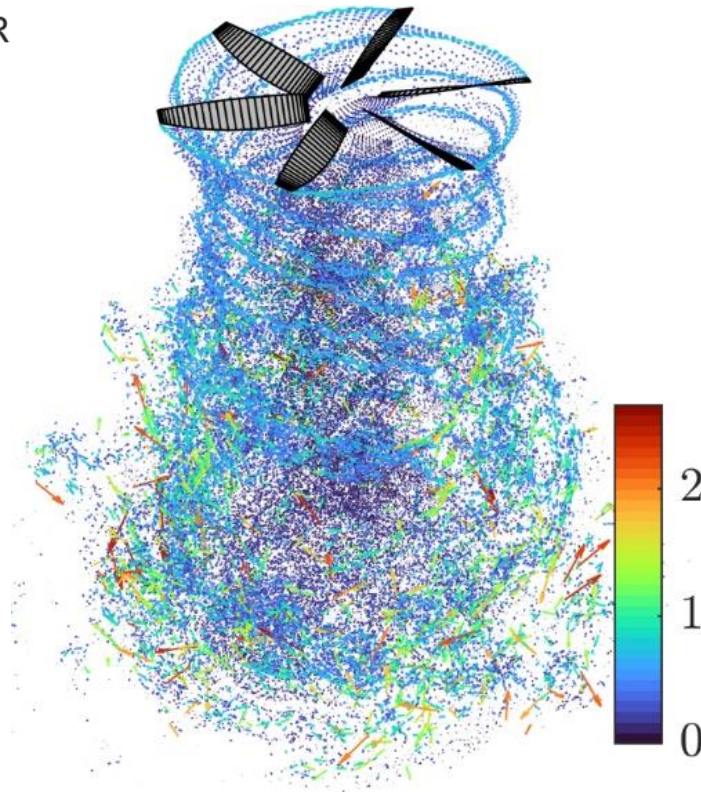
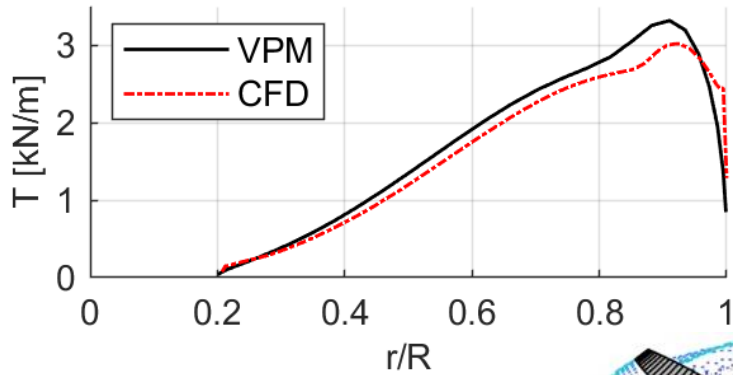
Vehicle geometry

- Reproduced in OpenVSP
- $R = 3.25m$
- DegenGeom used to export surface panelling



Isolated rotor case

- VPM over-predicts integrated thrust by 7.1%.

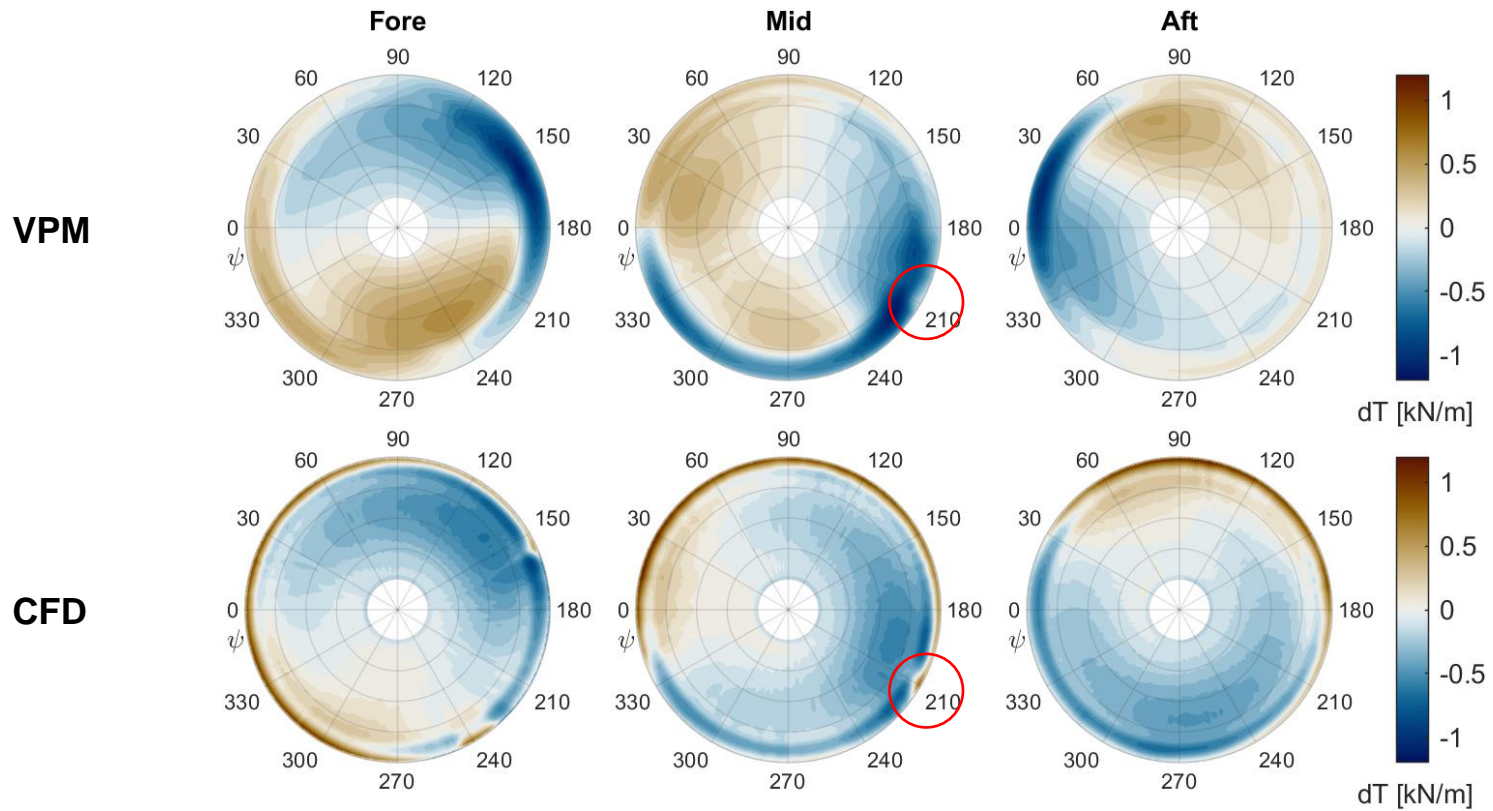


Multi-propeller case: averaged loads

- Within 6% of the CFD result.
- Including wings has small effect.

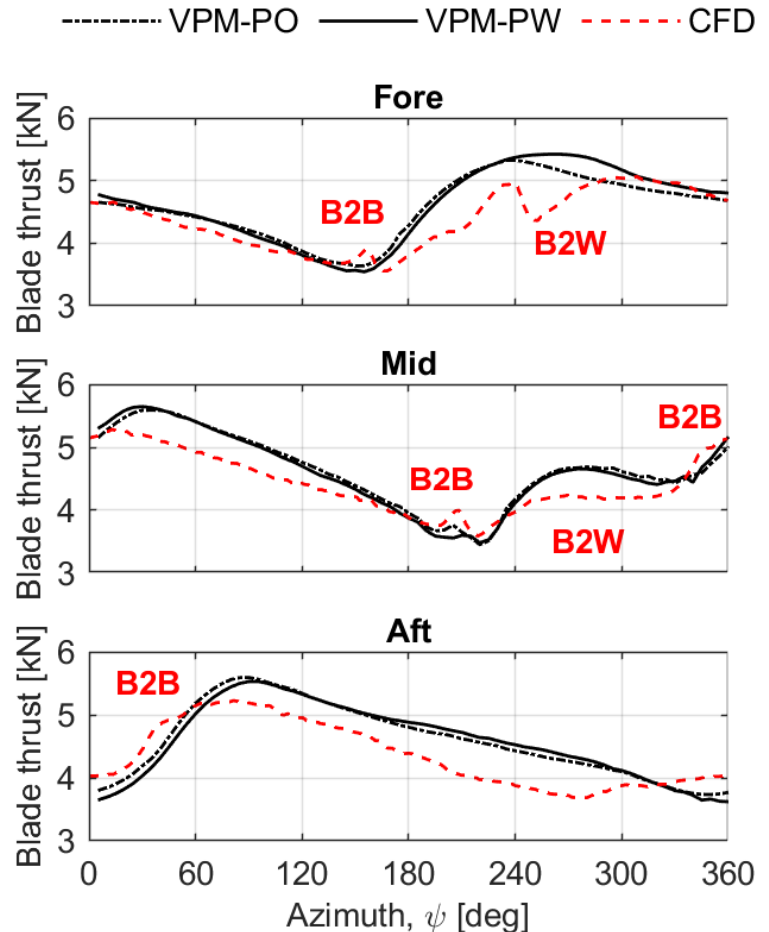
Case	\bar{T} [kN] Fore	\bar{T} [kN] Mid	\bar{T} [kN] Aft
VPM-PO	27.4	27.8	27.6
VPM-PW	27.7	27.7	27.5
CFD	26.2	26.5	26.2

Thrust distribution

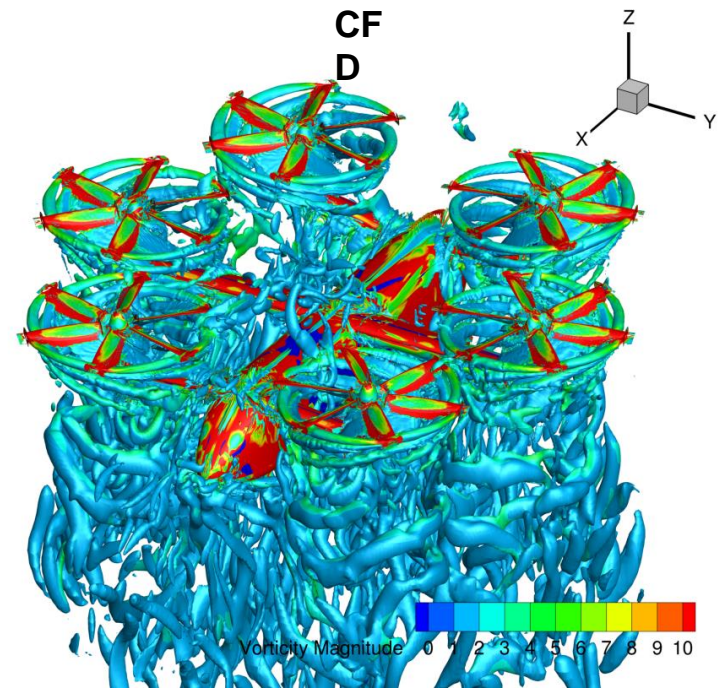
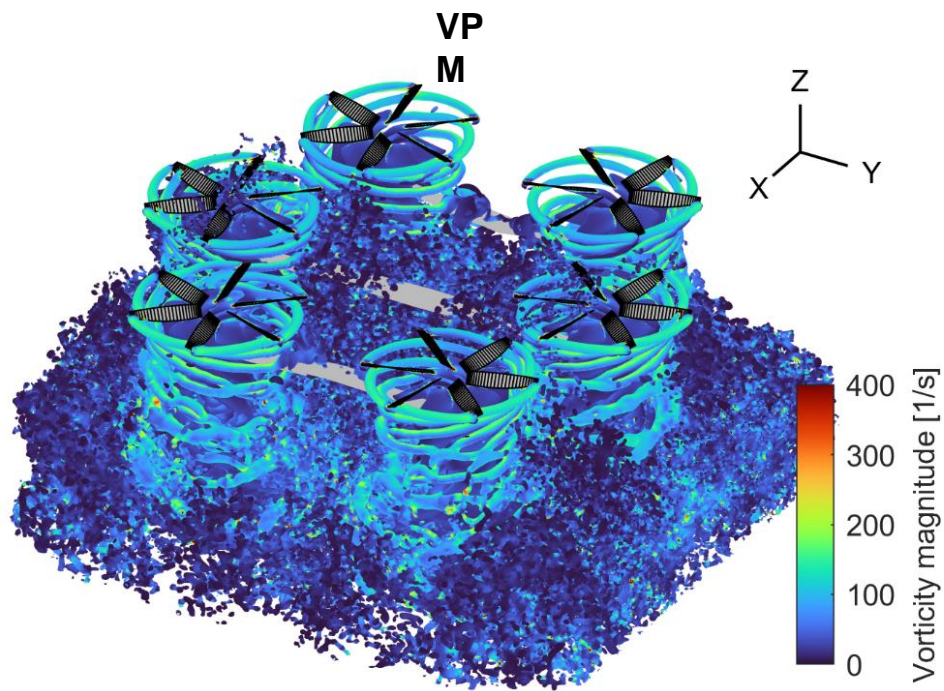


Blade loads

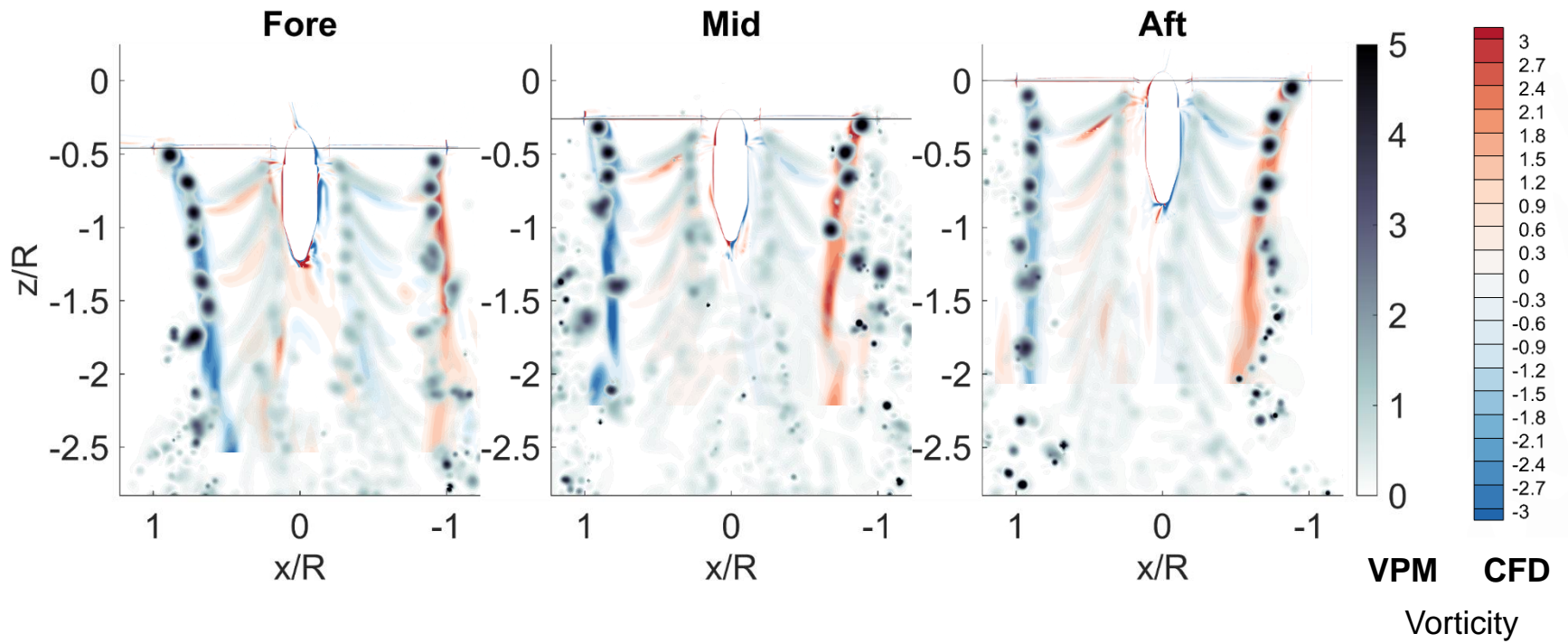
- Averaged over all blades
- 1/rev variation agrees well
- Blade-blade (B2B), blade-wing (B2W) interactions less well resolved.



Wake development, 6 rotors



Zhang et al. (J. Sound & Vibr. 2024)



Computing times

- Averaged thrusts within 6% of CFD solutions
- 4,000 vs 100,000 CPU hours
- Blade 1/rev thrust variation well captured
- Smaller-scale blade-blade, blade-wing interactions less well resolved
- (Analytical model: instantaneous solutions)

Summary

- Full computational capability
- Some experimental capability

Vortex particle method

- Vorticity form of the incompressible Navier-Stokes equation

$$\frac{D}{Dt} \boldsymbol{\omega} = (\boldsymbol{\omega} \cdot \nabla) \mathbf{u} + \nu \nabla^2 \boldsymbol{\omega}$$

- Vorticity field is discretised into vortex particles with core radius σ and strength α

$$\boldsymbol{\omega}(\mathbf{x}, t) \approx \sum_p \alpha_p(t) \zeta_\sigma(\mathbf{x} - \mathbf{x}_p(t))$$

Gaussian cut-off function $\zeta_\sigma(\mathbf{r}) = \frac{1}{\sigma^3} \frac{3}{4\pi} e^{-\left(\frac{\mathbf{r}}{\sigma}\right)^3}$

Vortex particle method

- Velocity field induced by particles according to the Biot-Savart law with a regularised kernel

$$\mathbf{u}(\mathbf{x}, t) = \sum_p g_\sigma(\mathbf{x} - \mathbf{x}_p(t)) \mathbf{K}(\mathbf{x} - \mathbf{x}_p(t)) \times \boldsymbol{\alpha}_p(t),$$

with singular kernel $\mathbf{K}(\mathbf{r}) = -\frac{\mathbf{r}}{4\pi r^3}$

and regularisation function

$$g_\sigma(\mathbf{r}) = 1 - e^{-\left(\frac{r}{\sigma}\right)^3}$$

Particle evolution equations

- The **reformulated** vortex particle method of Alvarez, Mehr and Ning (AIAA, 2022) introduces an additional degree of freedom $\frac{d}{dt} \sigma_p$ to enforce momentum and mass conservation.

- Advection: $\frac{d}{dt} \mathbf{x}_p = \mathbf{u}(\mathbf{x}_p)$
- Stretching: $\frac{d}{dt} \boldsymbol{\alpha}_p = (\boldsymbol{\alpha}_p \cdot \nabla) \mathbf{u}(\mathbf{x}_p) - \frac{g+f}{\frac{1}{3}+f} \{[(\boldsymbol{\alpha}_p \cdot \nabla) \mathbf{u}(\mathbf{x}_p)] \cdot \hat{\boldsymbol{\alpha}}_p\} \hat{\boldsymbol{\alpha}}_p + \frac{d\boldsymbol{\alpha}_p}{dt} \Big|_{visc}$
- Core size: $\frac{d}{dt} \sigma_p = -\frac{g+f}{1+3f} \frac{\sigma_p}{\|\boldsymbol{\alpha}\|_p} [(\boldsymbol{\alpha}_p \cdot \nabla) \mathbf{u}(\mathbf{x}_p)] \cdot \hat{\boldsymbol{\alpha}}_p$

$g = 1/5, f = 0$ used for the reformulated method

$g = 0, f = 0$ recovers the classic evolution equations

Boundary Element Method

- Source panels used to model solid surfaces.
- Dirichlet BC.
 - Simultaneously solve for flow tangency on all vortex panel and source panel centroids.
 - Obtain vortex and source strengths.

Blade model: Lifting line

- Blade is discretised span-wise into panels.
- The circulation of each panel is solved by enforcing flow-tangency at the panel centroids, with Prandtl-Glauert compressibility correction.
- The inviscid loads on each panel are calculated based on their circulation, Γ :

$$d\mathbf{F} = \rho\Gamma(\mathbf{u} \times d\mathbf{l}) + \rho c \frac{\partial\Gamma}{\partial t} \hat{\mathbf{n}}$$

- Profile drag is corrected post-solution from aerodynamic look-up tables.
- For low-Re cases, lift coefficient can also be corrected from look-up tables based on calculated effective angle of attack.
 - Must be coupled to the blade circulation.
 - Can be costly to obtain convergence, prone to instabilities.